

THE VIEWS AND CONCLUSIONS CONTAINED IN THIS DOCUMENT ARE THOSE OF THE AUTHORS AND SHOULD NOT BE INTERPRETED AS NECESSARILY REPRESENTING THE OFFICIAL POLICIES, EITHER EXPRESS OR IMPLIED, OF THE DEFENSE ADVANCED RESEARCH PROJECTS AGENCY OR THE U. S. GOVERNMENT.

LEVEL II

12

B5

AD A 099 124

**VISIBLE LASER RESEARCH
ONE-METER DEVICE**

**D. Trainor and H. Hyman, et al.
Avco Everett Research Laboratory, Inc.
2385 Revere Beach Parkway
Everett, MA 02149**

Final Technical Report for Period 23 August 1976 to 1 April 1981

**DTIC
ELECTE
S MAY 18 1981**

E

APPROVED FOR PUBLIC RELEASE; DISTRIBUTION UNLIMITED.

Sponsored by

**DEFENSE ADVANCED RESEARCH PROJECTS AGENCY
DARPA Order No. 3125**

Monitored by

**OFFICE OF NAVAL RESEARCH
DEPARTMENT OF THE NAVY
Arlington, VA 22217**

DTIC FILE COPY

81 5 18 059

FOREWORD

DARPA Order No.: 3125

Contractor: Avco Everett Research Laboratory, Inc.

Effective Date of Contract: August 23, 1976

Contract Expiration Date: April 1, 1981

Contract No.: N00014-76-C-1032

Short Title of Work: One-Meter Device

Principal Investigator and Phone No.: D.W. Trainor
(617) 389-3000, Ext. 467

Scientific Officer: Director Physics Program
Physical Science Division
Office of Naval Research
800 North Quincy Street
Arlington, VA 22217

Amount of Contract: \$1,976,642

UNCLASSIFIED

SECURITY CLASSIFICATION OF THIS PAGE (When Data Entered)

REPORT DOCUMENTATION PAGE		READ INSTRUCTIONS BEFORE COMPLETING FORM
1. REPORT NUMBER	2. GOVT ACCESSION NO. AD-A099124	3. RECIPIENT'S CATALOG NUMBER
4. TITLE (and Subtitle) 6. VISIBLE LASER RESEARCH ONE-METER DEVICE,	5. TYPE OF REPORT & PERIOD COVERED 9. FINAL TECHNICAL REPORT, 23 Aug. 1976-1 April 1981	6. PERFORMING ORG. REPORT NUMBER
7. AUTHOR(s) 10. D. Trainor, H. Hyman, J. Hsia J. Jacob, C. Duzy and M. Rokni	8. CONTRACT OR GRANT NUMBER(s) 15. N00014-76-C-1032 ✓ DARPA Order-3125	
9. PERFORMING ORGANIZATION NAME AND ADDRESS Avco Everett Research Laboratory, Inc. 2385 Revere Beach Parkway Everett, MA 02149	14. PROGRAM ELEMENT, PROJECT, TASK AREA & WORK UNIT NUMBERS 11. 1981	
11. CONTROLLING OFFICE NAME AND ADDRESS Defense Advanced Research Projects Agency DARPA Order No. 3125	12. REPORT DATE	
14. MONITORING AGENCY NAME & ADDRESS (if different from Controlling Office) Office of Naval Research Department of the Navy Arlington, VA 22217	13. NUMBER OF PAGES 79 1283	15. SECURITY CLASS. (of this report) Unclassified
16. DISTRIBUTION STATEMENT (of this Report) Approved for public release; distribution unlimited.		15a. DECLASSIFICATION/DOWNGRADING SCHEDULE
17. DISTRIBUTION STATEMENT (of the abstract entered in Block 20, if different from Report)		
18. SUPPLEMENTARY NOTES		
19. KEY WORDS (Continue on reverse side if necessary and identify by block number) KrF, XeF, HgCl₂, Stimulated Raman Scattering, Blue-Green, Hydrogen		
20. ABSTRACT (Continue on reverse side if necessary and identify by block number) This final report summarizes research results obtained at Avco on a one-meter laser device. This apparatus was originally designed and constructed to be a useful scaling device for evaluation of the performance characteristics of the then recently discovered rare gas halide laser candidates. Sub- sequently, under this contract, a large number of technical achievements have been attained which have advanced the under-		

DD FORM 1 JAN 73 1473

EDITION OF 1 NOV 65 IS OBSOLETE

048450

UNCLASSIFIED
SECURITY CLASSIFICATION OF THIS PAGE (When Data Entered)

UNCLASSIFIED

SECURITY CLASSIFICATION OF THIS PAGE(When Data Entered)

20. standing of various laser systems. These accomplishments have provided DARPA/ONR with very useful information for the evaluation of these lasers for a variety of mission applications.

UNCLASSIFIED

SECURITY CLASSIFICATION OF THIS PAGE(When Data Entered)

TABLE OF CONTENTS

<u>Section</u>	<u>Page</u>
List of Illustrations	3
I. INTRODUCTION	7
A. KrF Laser ($\lambda=249$ nm)	8
B. XeF Laser ($\lambda=350$ nm)	9
C. Blue-Green Laser Studies	10
1. HgCl ($\lambda = 588$ nm)	10
2. Raman Conversion of XeF	11
II. BLUE-GREEN CONVERSION OF XeF USING STIMULATED RAMAN SCATTERING TECHNIQUES	13
A. Background	13
B. Experimental Results (U)	25
1. Short-Pulse Laser Experiments: Lumonics XeF Laser	25
2. Long-Pulse Laser Experiments: 1-Meter E-Beam Pumped Laser	51

Accession For	
NTIS GRA&I	<input checked="" type="checkbox"/>
DTIC TAB	<input type="checkbox"/>
Unannounced	<input type="checkbox"/>
Justification	
By _____	
Distribution/	
Availability Codes	
Dist	Avail and/or Special
A	

LIST OF ILLUSTRATIONS

<u>Figure</u>		<u>Page</u>
1	Optical Conversion by Stimulated Raman Scattering	14
2	Blue-Green Wavelengths Accessible by Stimulated Raman Scattering (SRS) of XeF, XeCl and KrF with H ₂	16
3	Potential Energy Curves Depicting Non-Resonant Features of XeF Pumped SRS Processes in Hydrogen	17
4	Pressure Effect of H ₂ Raman Linewidth	18
5	Model Predictions for Cell Length Variations and Their Influence on the Resulting Stokes Shifts for Ruby Laser Pumped CS ₂	20
6	Two-step two-cell Raman Conversion to the Blue-Green	22
7	Combination Schemes for Four-Wave Parametric Processes	23
8	Schematic of Experimental Setup where L is the Lumonics Laser, a and b are 50 cm fl lens, C is the High-Pressure Cell, D is a Photodiode, F are Filters and O is a Spectral Monitoring or Energy Measuring Device	27
9	Focal Length Profiles	29
10	Energy Measured Through a 0.05 cm Pinhole vs Distance from Focus	30
11	Various Laser Output Photons vs Total H ₂ Pressure	32
12	Optimized XeF Conversion to First Stokes vs Input Energy	33
13	First Stokes Gain for Forward SRS in H ₂ . Solid line is wavelength-scaled calculation normalized to Bloembergen's result with ruby; *indicates the value deduced from this work	35

<u>Figure</u>		<u>Page</u>
14	XeF lasing Transitions	36
15	Temporal Characteristics of First Stokes (H_2) Spectral Lines Using the Short Focal Geometry	38
16	Schematic of Experimental Setup Where C_1 and C_2 are the Two High-Pressure Cells and P_1, P_2 the Photodiodes for Monitoring the Inputs to each Cell Respectively	41
17	Energy Measured Through 0.05 or 0.04 cm Diameter Pinholes vs Distance from Focus for S_1 Radiation	44
18	Cell 2 (H_2, H_2) Pressure Variation Effect on S_1 Pump and the Generation of S_2	45
19	Cell 2 Threshold for S_2 as a Function of S_1 Input Intensity	47
20	Pulse Temporal Narrowing in Successive Conversion	48
21	Two-Step KrF/ D_2/H_2 Raman Conversion	50
22	Spectra Giving Qualitative Indication of Relative Intensities of XeF Pumped H_2 (AS_1, P, S_1, S_2)	52
23	Blue-Green Optical Conversion of XeF* (1 Meter Device)	54
24	Photograph of 1-m Xenon Fluoride Laser	56
25	Stimulated Raman Output from XeF Pumped H_2	57
26	Experimental Parameters Used to Explore Raman Process	58
27	First Stokes Gain for Forward SRS in H_2	60
28	SRS Threshold Data (1.35 m Focus: 26 atm H_2)	62
29	Energy Conversion Measurement Experimental Setup	63
30	Significant S_3 Production at Hard Focus (1.35 m) Plot of S_n/S_1 vs H_2 Pressure	66
31	Reduced S_3 Production at Softer Focus (3.6 m) Plot of S_n/S_1 vs H_2 Pressure	67

<u>Figure</u>		<u>Page</u>
32	S_1 Dominates at Soft Focus (4.6 m) Plot of S_n/S_1 vs H_2 Pressure	68
33	Pressure Insensitive S_1 and S_2 Output at Softest Focus Studied (5.1 m), Plot of S_n/S_1 vs H_2 Pressure	69
34	SRS Threshold Behavior (3.6 m focus)	70
35	Raman Temporal Signals Observed at Soft Focus (4.6 m) Showing Pump Depletion of ~ 70%	71
36	Raman Temporal Signals Observed at Softest Focus Studied (5.1 m) Showing Pump Depletion of ~ 72%	72
37	Different Thresholds Observed for S_1 and S_2 at 5.1 m Focal Arrangement	73
38	Spatial Beam Profile Influence on Raman Output	75
39	Spectrographic Evidence for Focal Length Influence on Minimizing Parametric Processes	78

I. INTRODUCTION

Many contributions to the understanding of the physics and scaling limitations of rare gas halide and mercury halide lasers have been generated as part of this DARPA/ONR sponsored research program.

In carrying out this research, a sequence of experimental investigations was typically performed in the following order. New laser candidates were initially lased on a small-scaled e-beam device. These newly discovered lasers were then subsequently investigated on a small-scale, cable-driven e-beam under experimental conditions which were selected: to determine the formation processes by both e-beam and discharge pumping, to determine the quenching kinetics, to measure gain and absorption, and often to explore the effects of elevated temperature on the laser's performance characteristics. This kinetic data base was then used to develop and refine a laser code with predictive capability with regard to laser performance under power extraction. These code predictions were then tested by comparison to the laser's performance on the 1-m device that was constructed under this contract. This then allowed projections to be made for a variety of DARPA/ONR mission objectives.

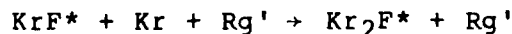
Using this approach, scaling issues for a number of laser candidates were explored in detail. A complete description of the

results of these early investigations is available in prior Semi-Annual and Interim Technical Reports (Ref. 1). A brief summary highlighting these research results is listed below.

A. KrF LASER ($\lambda=249$ nm)

Krypton fluoride was the earliest rare gas halide laser that was subjected to intense investigation under this program. Small-scale experiments suggested it was efficient and volumetrically scalable. As part of this program, the following significant results were obtained:

- Important KrF* formation and quenching rates were measured.
- Kr₂F* formation in KrF* laser mixtures was shown to occur predominantly from reactions involving KrF* as a precursor and consequently was saturable with cavity flux.
- Rate constants for three-body recombination reactions of the type



were calculated as a function of temperature.

- Use of these rates in a kinetics model enabled us to predict KrF* laser performance.
- Using e-beam pumping, a laser output energy of 102 J with an active laser volume of 8.5 ℓ (12J/ℓ) at an intrinsic efficiency of 9% was obtained.
- Using e-beam controlled discharge excitation of KrF*, a laser output energy of 75 J was obtained in an active volume of 7.5 ℓ (10 J/ℓ) at an intrinsic efficiency of 10%. The discharge enhancement ratio (discharge energy into the medium/e-beam energy absorbed in the medium) was 2.

1. Hsia, J.C., Jacob, J.H., Mangano, J.A. and Rokni, M., Semi-Annual Technical Report: Aug. 76 - Feb. 77, Feb. 77 - Aug. 77, Nov. 77 - May 78; Hsia, J.C., Jacob, J.H. and Duzy, C., Semi-Annual Technical Report May 78 - Feb. 79; Trainor, D.W. and Hyman, H.A., Interim Technical Report, July 79 - Feb. 80.

- The laser output, KrF*, and Kr₂F* sidelight intensities were measured and shown to agree with model predictions.
- KrF laser scaling projections were made.
- KrF* and Kr₂F* fluorescence was measured as a function of temperature. The results were consistent with the calculated temperature dependence of the three-body quenching of KrF* by Ar and Kr.
- The KrF intrinsic laser efficiency was shown to improve with temperature.

B. XeF LASER ($\lambda=350$ nm)

Xenon fluoride subsequently became the leading rare gas halide laser candidate for continued DARPA funded research due to its longer operating wavelength, which makes it potentially useful for applications involving atmospheric propagation. The following results were obtained:

- Important XeF* formation and quenching rates were measured.
- An XeF* formation chain in neon rich mixtures was proposed and shown to be consistent with all experimental observations.
- XeF* formation was shown to proceed with unit branching in e-beam excited argon and neon rich mixtures.
- Using pure e-beam excitation, an XeF* laser output of 36 J was obtained in an active volume of 4.5 l (8J/l) at an intrinsic efficiency of 2.6%.
- This laser efficiency was shown to be limited by the slow vibrational mixing in the upper level manifold and bottlenecking in the lower level.
- Elevated temperature was identified as a technique for improving XeF laser efficiency; subsequently its intrinsic efficiency was shown to increase by more than a factor or two at elevated temperature ($\sim 450^\circ\text{K}$).
- This increase in laser efficiency was shown to be a result of improved energy extraction brought about by an

increased rate of lower level removal and upper state vibrational mixing.

- The change in output spectra (from $\lambda=353$ to $\lambda=351\text{nm}$) at elevated temperatures was shown to be attributable to the increase in lower level removal and a change in upper state rotational distribution.
- The energy loss due to the formation of the $\text{XeF}^*(\text{C})$ state and excited triatomics in XeF laser mixtures was shown to be saturable by laser cavity flux.
- The rates of lower state ($\text{XeF}(\text{X})$) removal by vibrational mixing and dissociation were calculated for various vibrational states and temperatures.
- The various effects of increased temperature in XeF laser kinetics were incorporated into the comprehensive laser model.
- An XeF laser specific energy of 14 J/l was achieved at 3 amagats (4.7 J/l-Amg) with 5% intrinsic efficiency.
- The observed laser performance was shown to be consistent with model predictions.

C. BLUE-GREEN LASER STUDIES

Research has also been conducted to explore efficient blue-green laser candidates as to their suitability for strategic laser communication applications. There have been two studies directly pursued under this program. The first involved HgCl , whereas more recent research has been carried out exploring the technique of stimulated Raman scattering of XeF radiation in molecular hydrogen.

1. HgCl Laser ($\lambda = 588 \text{ nm}$)

The initial laser demonstrations were carried out using direct e-beam excitation, where the efficiency was found to be low predominantly due to the low HgCl^* production efficiency by direct

e-beam pumping. Under this program, alternative excitation techniques (e-beam discharge) were considered. The results obtained were as follows:

- E-beam controlled discharge experiments were carried out in Hg/Cl₂/Ar mixtures with no pre-reaction between mercury and chlorine.
- The measured small signal gain and fluorescence efficiency under optimum laser conditions suggested poor HgCl* formation from two of the three Hg* metastable sub-levels (i.e., ³P₀, ³P₁) as a result of "harpooning" reactions with Cl₂.
- Active medium photoabsorption of Hg/Cl₂/Ar mixtures near the laser wavelength was measured using a probe laser and found to be large (0.4 to 0.8%/cm) under typical operating conditions.
- A HgC intrinsic laser efficiency of 3% was obtained with a discharge enhancement ratio of 11.
- The results of these HgCl* laser experiments were compared with model calculations with good agreement.

2. Raman Conversion of XeF

With regard to the stimulated Raman scattering experimental program, a brief list of the major accomplishments is included below.

- In small-scale experiments, 66% power conversion efficiencies of XeF pump radiation to first Stokes was observed.
- In large-scale experiments, using a 1-m laser as a pump, over 60% energy conversion of XeF to Raman output was observed.

A complete description of our Raman approach, the experimental techniques employed, and the results obtained under this contract are the main subject of this final report.

II. BLUE-GREEN CONVERSION OF XeF USING STIMULATED RAMAN SCATTERING TECHNIQUES

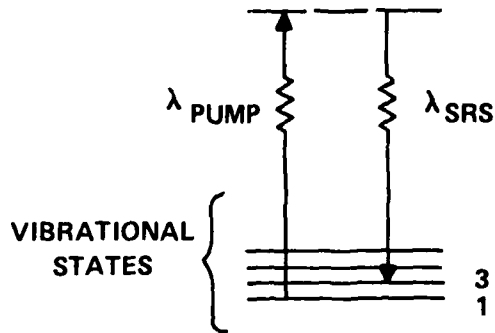
A. BACKGROUND

Stimulated Raman scattering (SRS) involves an inelastic scattering mechanism in which a photon incident on an atom or molecule causes the atom or molecule to undergo a change in internal energy and emit a photon that is shifted in wavelength from the incident photon by that exact change in internal energy. In the case of an atom, the internal energy is in the form of an electronic transition (see Figure 1). For a molecule, the change in internal energy can be vibrational or rotational.

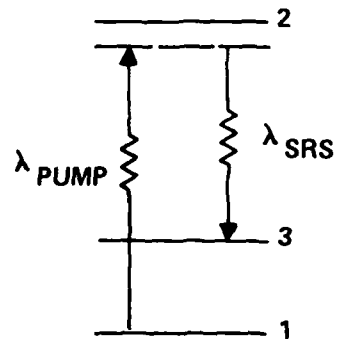
The electronic Raman process can achieve large wavelength shifts in a single step but, specifically for this blue-green application, utilizing efficient, ultraviolet excimer lasers as pumps, the scattering atoms are high-temperature metal vapors (e.g., XeCl shifted lead). These approaches thereby suffer from the technology problems associated with the production of the atom source. The molecular Raman process, on the other hand, utilizes a room temperature, chemically inert gas, but suffers from a small Stokes shift which is identical to the vibrational spacing. Since hydrogen has the largest vibrational energy

MOLECULAR SRS

————— 2



ATOMIC SRS



H8443

Figure 1 Optical Conversion by Stimulated Raman Scattering

spacing, it is a leading contender to shift to the blue-green in a minimum number of steps using the various ultraviolet excimer lasers available as possible pumps (see Figure 2).

From practical considerations (as to the number of shifts, the efficiency of the pump and the quantum yields involved), we identified XeF/H₂ as the preferred process. This Raman process involves a very nonresonant transition (see Figure 3) and has, therefore, a small Raman cross section (relative to the atomic case) and experiments are typically carried out at high pressure. In fact, pressure is one of the most significant parameters affecting the molecular SRS process. This is because the variation in pressure will affect both the number density of the scatterer and the spontaneous Raman linewidth. Since the gain is equal to the Raman cross section times the density times the length, i.e.,

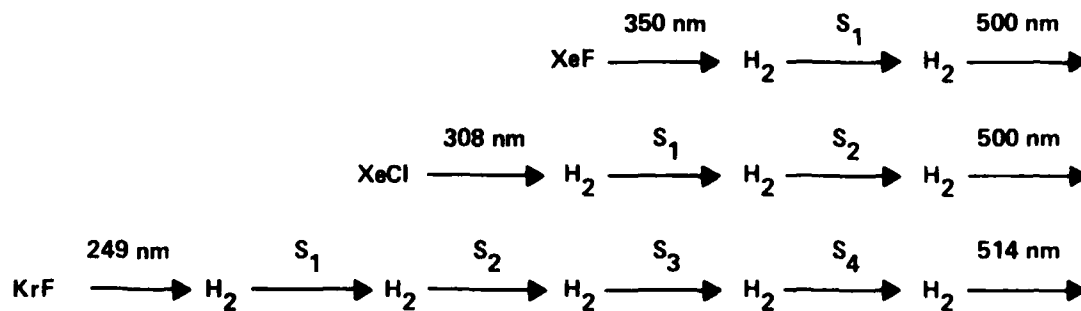
$$\text{GAIN} = \sigma \text{NL}$$

and the Raman cross section is inversely proportional to the Raman linewidth, a consideration of the pressure influence on the gain is important.

There are three distinct pressure regimes (Ref. 2) for the H₂ Raman linewidth (see Figure 4). At very low pressures, the linewidth is primarily determined by Doppler broadening and is independent of pressure; therefore the gain is directly proportional to the pressure. At pressures near 0.3 atm, the forward scattering Raman line width decreases due to collision narrowing effects, resulting from the frequent velocity-changing but not

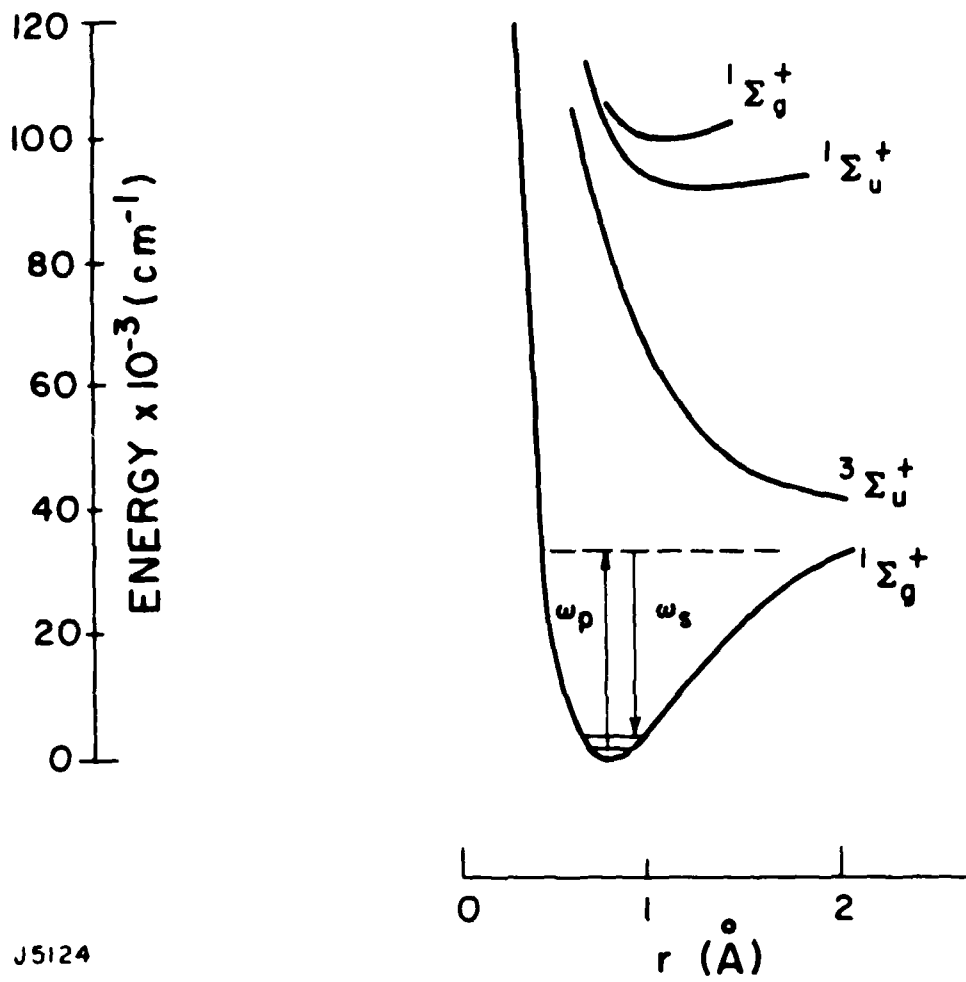
2. Murray, J.R. and Javan, A., J. Molec. Spectry. 42, 1, (1972).

HYDROGEN PROVIDES THE LARGEST MOLECULAR WAVELENGTH SHIFT (4155 cm^{-1})



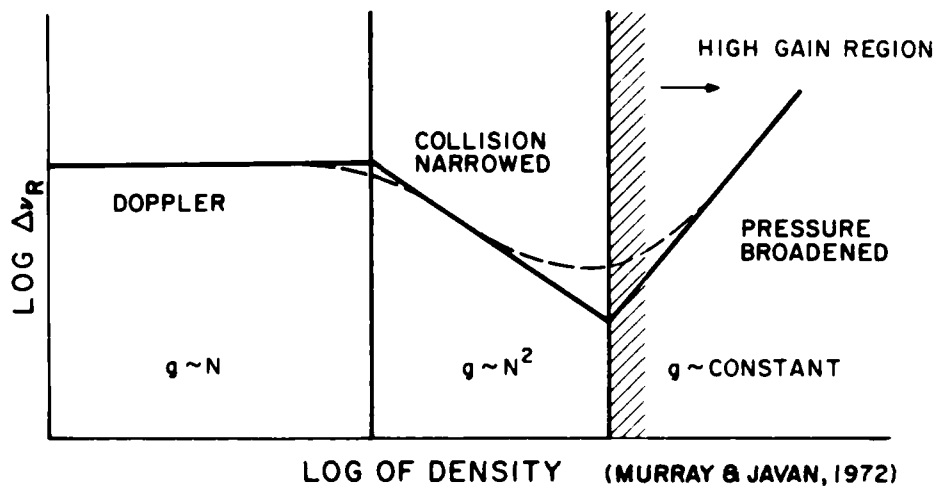
J6988

Figure 2 Blue-Green Wavelengths Accessible by Stimulating Raman Scattering (SRS) of XeF, XeCl and KrF with H₂



J5124

Figure 3 Potential Energy Curves Depicting Non-Resonant Features of XeF Pumped SRS Processes in Hydrogen



J6973

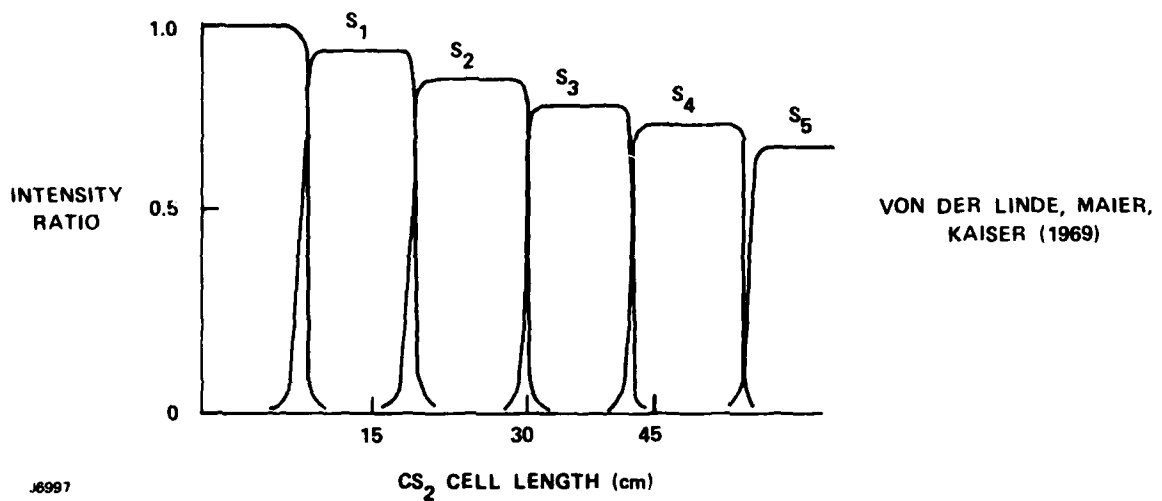
$$\text{GAIN} = \sigma NL \sim \frac{1}{\Delta\nu_R} NL$$

Figure 4 Pressure Effect of H₂ Raman Linewidth

phase-changing collisions. In this regime, the linewidth becomes inversely proportional to the density of the collision partner (i.e., H_2), and therefore, the gain scales as density squared. At still higher pressures ($\gtrsim 3$ atm), collision broadening effects increase the Raman linewidth and the Raman gain eventually becomes independent of pressure.

Studies of stimulated Raman scattering in hydrogen gas are numerous (Ref. 3) and a variety of pump lasers have been used in these previous experiments. In fact, stimulated Raman scattering in general has a rich literature associated with it and high conversion of pump photons to Raman output has been predicted theoretically, modeled extensively and observed experimentally (Ref. 4). Consider, for example, the model prediction in Figure 5. Here the pump laser was Ruby and the Raman scatterer was liquid CS_2 (Ref. 5). Through variations in the cell length, the

-
3. See for example: Minck, R.W., Terhune, R.W. and Rado, W.G., *App. Phys. Lett.* 3, 181, (1963), Demartini, F., and Ducuing, J., *Phys. Rev. Lett.* 17, 117 (1966), Bloembergen, N., Bret, G., Lallemand, P., Pine, A. and Sinova, P., *IEEE J. of Quant. Elect.* QE-3, 197 (1967), Venkin, G.V., Kulyuk, L.L. and Maleev, D.I., *Sov. J. Quant. Electron* 5, 1348 (1976), Loree, T.R., Sze, R.L., and Barker, D.L., *App. Phys. Lett* 31, 37 (1977), Wilke, V., and Schmidt, W., *App. Phys.* 18 177 (1979), Komine, H. and Stappaerts, E.A., *Optics Lett.* 4, 398 (1979) and Trainor, D.W., Hyman, H.A., Itzkan, I. and Heinrichs, R.M., *App. Phys. Lett* 37, 440 (1980).
 4. Murray, J.R., Goldhar, J., Emerl, D., and Szoke, A., *IEEE J. of Quant. Elect.* QE-15, 342 (1974)
 5. von der Linde, D., Maier, M. and Kaiser, W., *Phys. Rev.* 178, 178 (1969).



J6997

Figure 5 Model Predictions for Cell Length Variations and Their Influence on the Resulting Stokes Shifts for Ruby Laser Pumped CS_2

authors predicted and observed high conversion to arbitrary Stokes, essentially approaching unit photon conversion efficiency. In our experiments, which will be described below, we routinely converted > 60% of the energy of the pump to stimulated Raman output.

All of these literature sources and our own practical experience allowed us to confidently propose that xenon fluoride could be very efficiently shifted, using molecular hydrogen, to longer wavelengths. To insure that the desired Raman process dominated over other potential competing processes, we proposed that the shift to the blue-green from 350 nm be carried out in two distinct steps in two separate cells (see Figure 6). This was for two reasons: one involves wavelength selection by placing different scatterers in the two cells, e.g., H_2 and D_2 . In this way, different wavelengths across the blue-green region can be produced. The second reason involves the necessity of controlling a significant competitive process to stimulated Raman scattering for pump photons: parametric or four-wave processes (Ref. 6). These processes can occur when waves separated by a vibrational frequency copropagate in the Raman medium (see Figure 7). Different four-wave combinations can occur as long as phase matching and energy conservation are maintained.

The phase matching requirement implies that in a dispersive medium, the four-waves may not be able to couple in the axial direction. Experimentally, what is observed is the appearance of light at various Stokes and anti-Stokes shifted wavelengths in cones around the primary beam. To reduce significant parametric processes

6. Zhdanov, B.V., Kulyuk, L.L. and Pershin, S.M., Sov. J. Quant. Electron 6, 550 (1976).

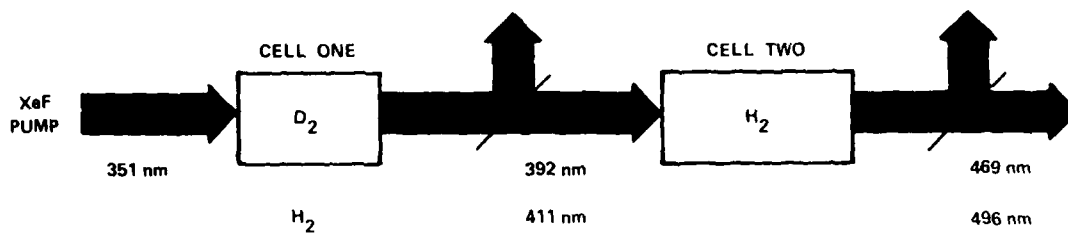
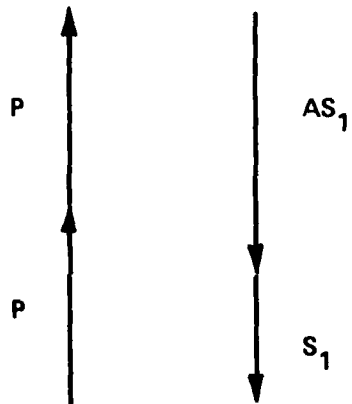
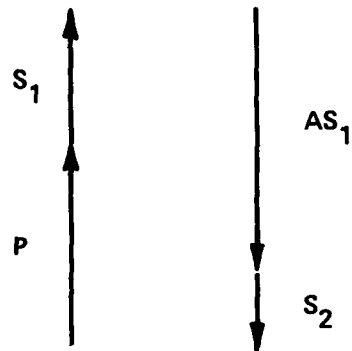


Figure 6 Two-step two-cell Raman conversion to the Blue/Green.



2 PUMP PHOTONS PRODUCE
STOKES AND ANTI-STOKES
PHOTONS



A STOKES AND PUMP PHOTON
PRODUCE ANTI-STOKES AND
2ND STOKES PHOTONS

J3759

Figure 7 Combination Schemes for Four-Wave Parametric Processes

from occurring, one can collinearly inject desired Stokes radiation with the pump, thereby reducing the likelihood of phase matching. In addition, since the number of potential parametric processes grows rapidly with the number of intense fields present, by restricting the conversion to a single Stokes shift in any one cell, the number of potential loss processes is reduced and control over the cell's output is enhanced.

B. EXPERIMENTAL RESULTS (U)

1. Short-Pulse Laser Experiments: Lumonics XeF Laser

From July 1979 to March 1980, we investigated efficient generation of Stokes shifted radiation using a commercial exciplex laser as the pump (Lumonics, TE-261-2) and molecular H_2 and D_2 as the Raman scattering media. General laser specifications as detailed by the manufacturer were found to be achievable with our particular device (e.g., it produced ~75 mJ of energy per pulse with XeF* and ~190 mJ for KrF* with the cavity optics provided). The beam quality associated with these achievable energies was insufficient to provide focused intensity-length products to achieve laser action in the Raman gas. We, therefore, altered the cavity optics to include Brewster windows and an unstable cavity configuration of the type described by Barker and Loree (Ref. 7). This cavity produced < 20 mJ of XeF laser energy in a pulse (FWHM) of ~6 ns with a beam waist ~10 times the diffraction limited value. The power density achievable was measured at the focus by recording the energy transmitted through various diameter pinholes. The beam waist at the focus of a 50 cm fl lens was found to be near 2.5×10^{-2} cm in diameter with an energy of 10 mJ. This, with the 6 ns pulselength, corresponds to an achievable power density of $\sim 3 \times 10^9$ W/cm² at the focus.

Efficient conversion however relies on an intensity-density-length product well in excess of threshold to achieve

7. Barker, D.L. and Loree, T.R., Appl. Opt. 16, 1192 (1977).

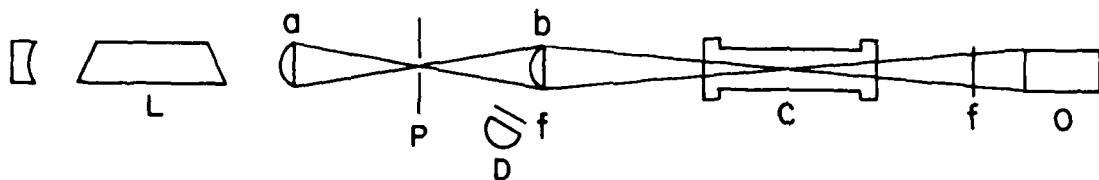
optimum conversion of XeF pump radiation to first Stokes. To measure efficiency and to parameterize the Raman process, the experimental setup shown in Figure 8 was used. Here the output of the Lumonics was focused through a pinhole to: 1) characterize the input beam, and 2) eliminate that portion of the pump with poor beam quality. In this arrangement, a second lens refocuses the beam into the center of our high-pressure Raman cell.

The Raman cells were constructed from available stainless steel shock tube sections about 40.6 cm long with an inner diameter of 3.8 cm and a wall thickness near 1.3 cm. The polished Dynasil quartz windows were near 6 cm in diameter and ~2.5 cm thick. The windows were supported by O-rings on the high-pressure side and by gaskets on the low-pressure side. The internal volume of these cells was near 465 cm³.

Pulse energies in these experiments were measured with a Scientech Model 362 energy/power meter. Pulse shapes were measured by photodiodes (ITT, type S-5 or Hamamatsu, type S-4). The outputs from the photodiodes were recorded by a Tektronics Model 7844 dual beam oscilloscope equipped with a C-51 oscilloscope camera.

Spectra were analyzed with either a 3/4 m monochromator, 1 m spectorgraph, or an optical multichannel analyzer (Tracor Northern, Model TN-1710, equipped with a Diode Array Rapid Scan Spectrometer).

SINGLE CELL EXPERIMENTS

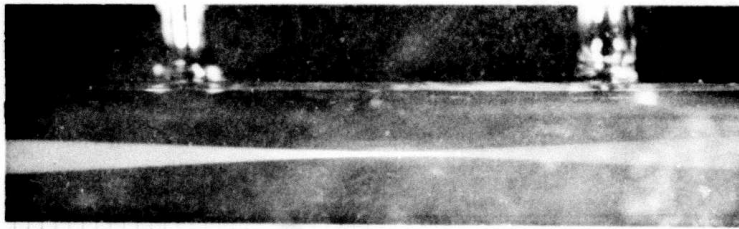


J3735

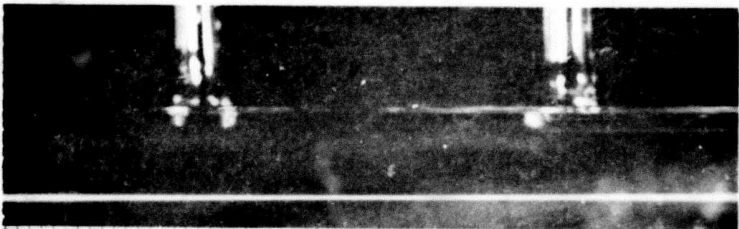
Figure 8 Schematic of Experimental Setup where L is the Lumonics Laser, a and b are 50 cm fL lens, C is the High-Pressure Cell, D is a Photodiode, F are Filters and O is a Spectral Monitoring or Energy Measuring Device

Using this arrangement and these various diagnostics, the effects of laser intensity, focal length, and H₂ pressure on the stimulated Raman scattering threshold, gain, Stokes production and conversion efficiency were investigated.

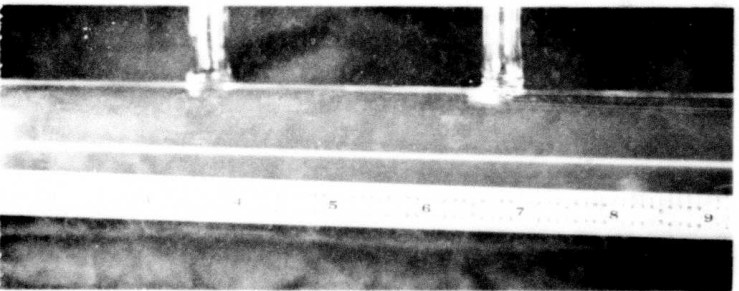
The pump laser intensity (at fixed focal length) was varied in two ways: by repeated firings to degrade the mix from optimum or by lowering the laser charging voltage. Using either technique, the subsequent results were identical, so the more convenient technique of varying the charging voltage was usually employed. Since these experiments were all carried out with focused geometry, a related factor to the intensity achieved (W/cm^2) is the length over which the intensity was high. A visual perspective of the various focal arrangements used is shown in Figure 9. These pictures were obtained by open shutter exposures of the focused laser light into a glass cell containing a dilute solution of Rhodamine 6 G. The focal length of ~135 cm geometry provided a beam waist of about 0.05 cm in diameter. Figure 10 shows a plot of the energy through this size pin-hole versus distance from focus. The distance between half-power points (or the effective Rayleigh range) is about 8 cm. Since the active length of the high-pressure cell is over 40 cm, there was no problem anticipated with gain clipping and no effect on the Raman output was observed when a Raman cell of ~90 cm was used.



20 cm FOCUS



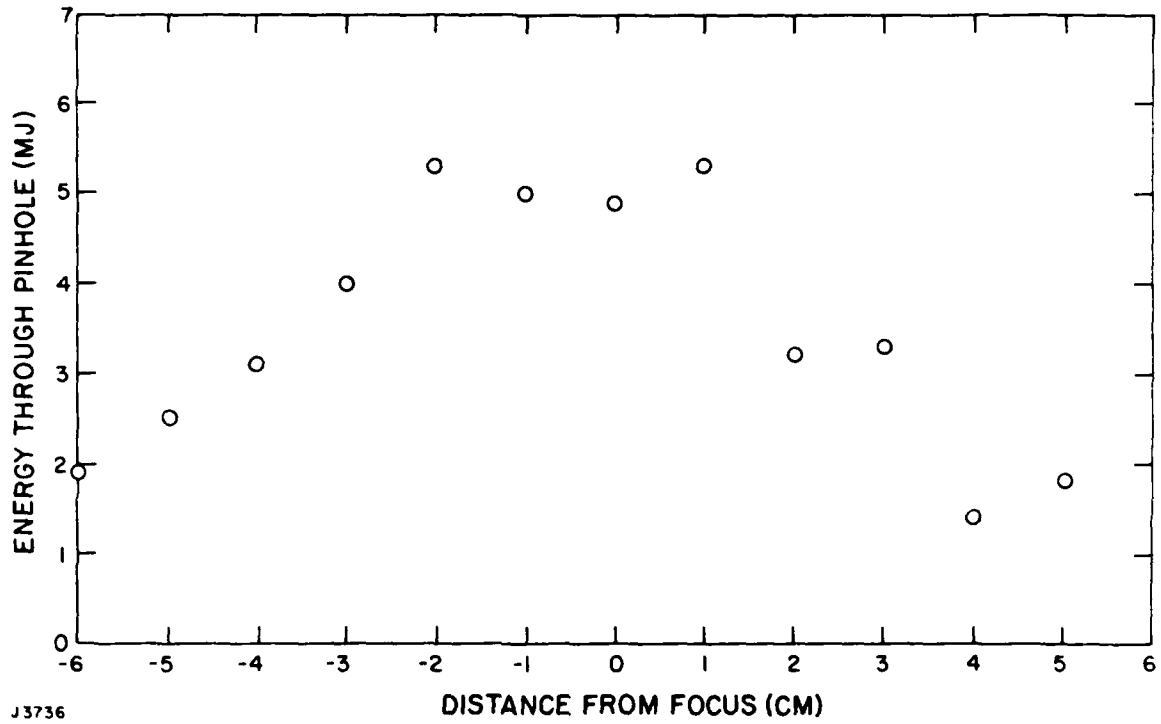
50 cm FOCUS



135 cm FOCUS

J3747

Figure 9 Focal Length Profiles



J3736

Figure 10 Energy Measured Through a 0.05 cm Pinhole vs Distance from Focus

For this experimental setup (at a maximum laser output corresponding to near 4.5×10^8 W/cm² for this relatively soft focal geometry), the dependence of forward scattered Stokes generation on H₂ pressure was measured (see Figure 11), using the optical multichannel analyzer (note that the intensity versus wavelength calibration had not been measured at this time). The first Stokes component appears to optimize at pressures above 15-20 atms (250 psi), whereas the second Stokes appears to peak near 25-30 atms and then decrease at higher pressures. These pressure scaling results are in agreement with the KrF/H₂ experiments of Loree (Ref. 8) and the gain saturation reported by Bloembergen (Ref. 9).

By now keeping the focal length and H₂ pressure fixed, variations in stokes output were measured as a function of XeF pump input, (see Figure 12). With data similar to these, it is possible to calculate the small-signal gain for this single-step process. From our measurements, we found threshold to be near 2.2 mJ. The pulse width was 6 ns and the length over which significant conversion occurred was near 8 cm with a beam waist at the center of the focal region of 0.05 cm. Since it is commonly regarded that a gain times length 30 is necessary to achieve lasing from noise (i.e., spontaneous Raman scattering), we can calculate the small-signal gain, g , as follows:

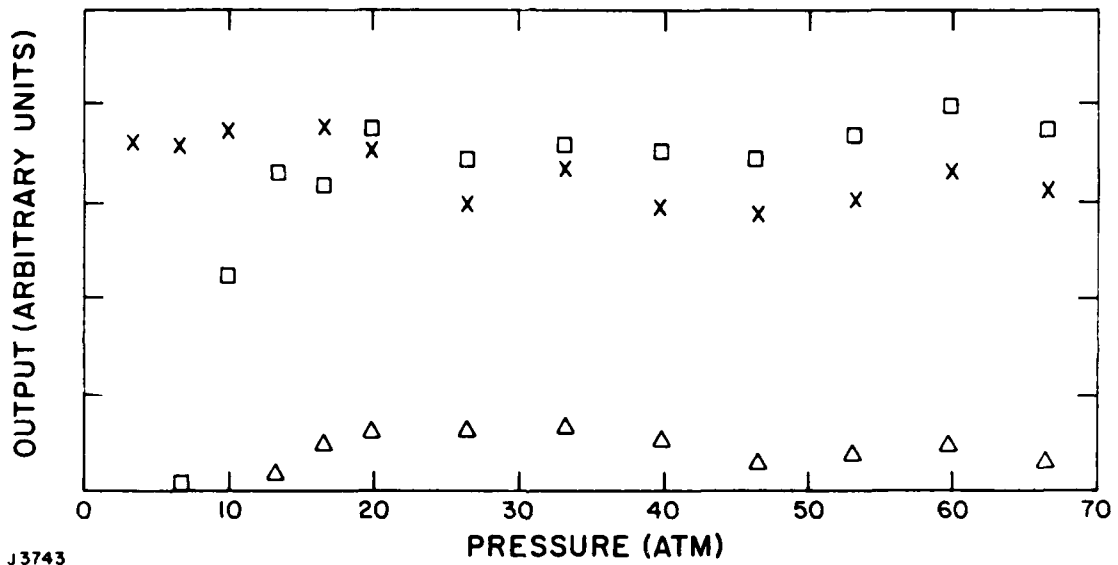
-
8. Loree, T.R., Sze, R.C. and Barker, D.L., App. Phys. Lett. 31, 37 (1977).
 9. Bloembergen, H., Bret, G., Lallemand, P., Pine, A. and Simova, P., IEEE J. Quant. Electron 3, 197 (1967).

H₂ PRESSURE VARIATION (Xe F)

X-DEPLETED PUMP

□-1st STOKES

△-2nd STOKES



J3743

Figure 11 Various Laser Output Photons vs Total H₂ Pressure

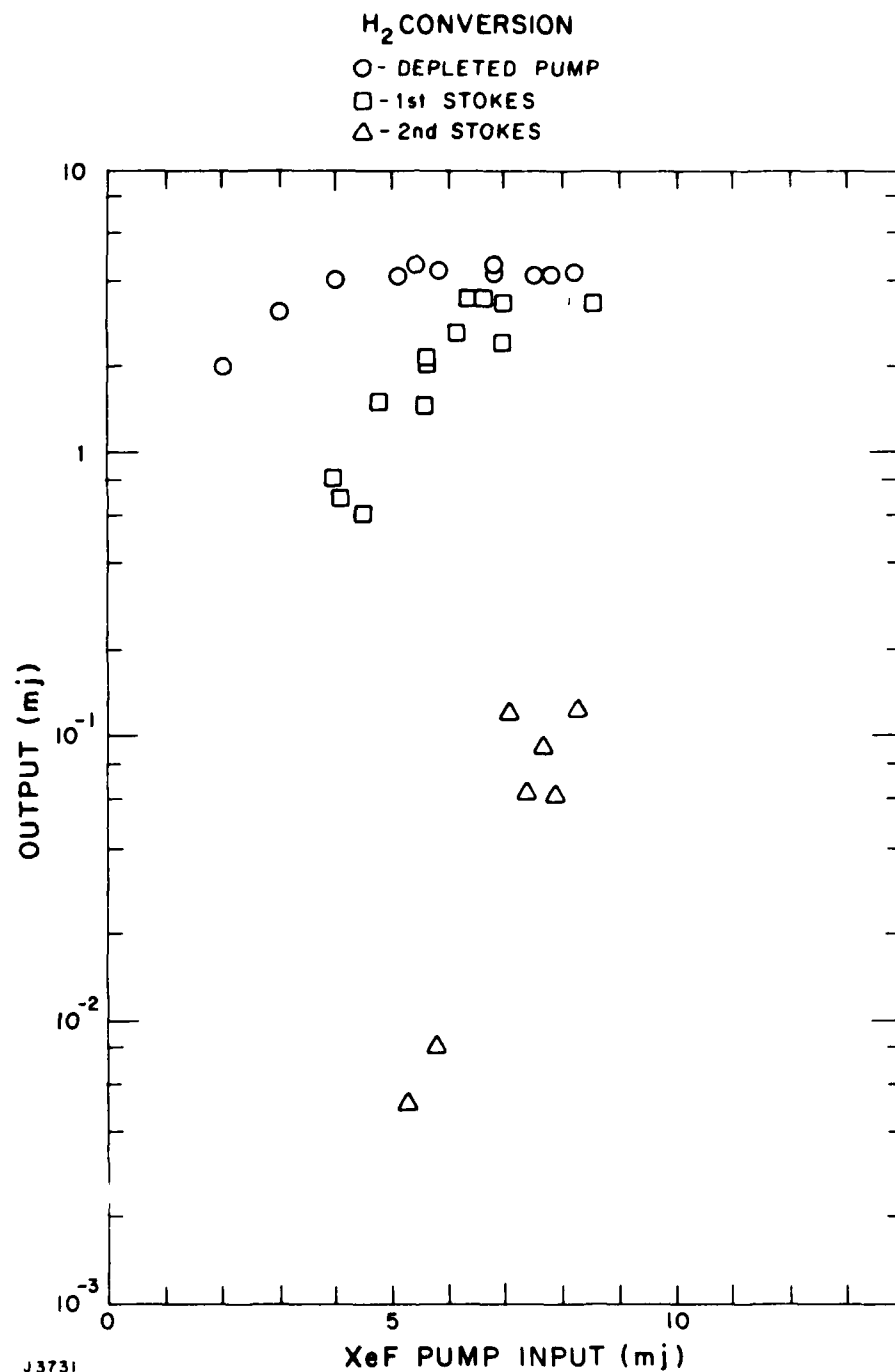


Figure 12 Optimized XeF Conversion to First Stokes vs Input Energy

$$g I_{Th} L \sim 30$$

where

$$I_{Th} = \frac{2.2 \times 10^{-3} \text{ J}}{6 \times 10^{-9} \text{ s} \times \pi (0.025 \text{ cm})^2} = 1.9 \times 10^8 \frac{\text{W}}{\text{cm}^2},$$

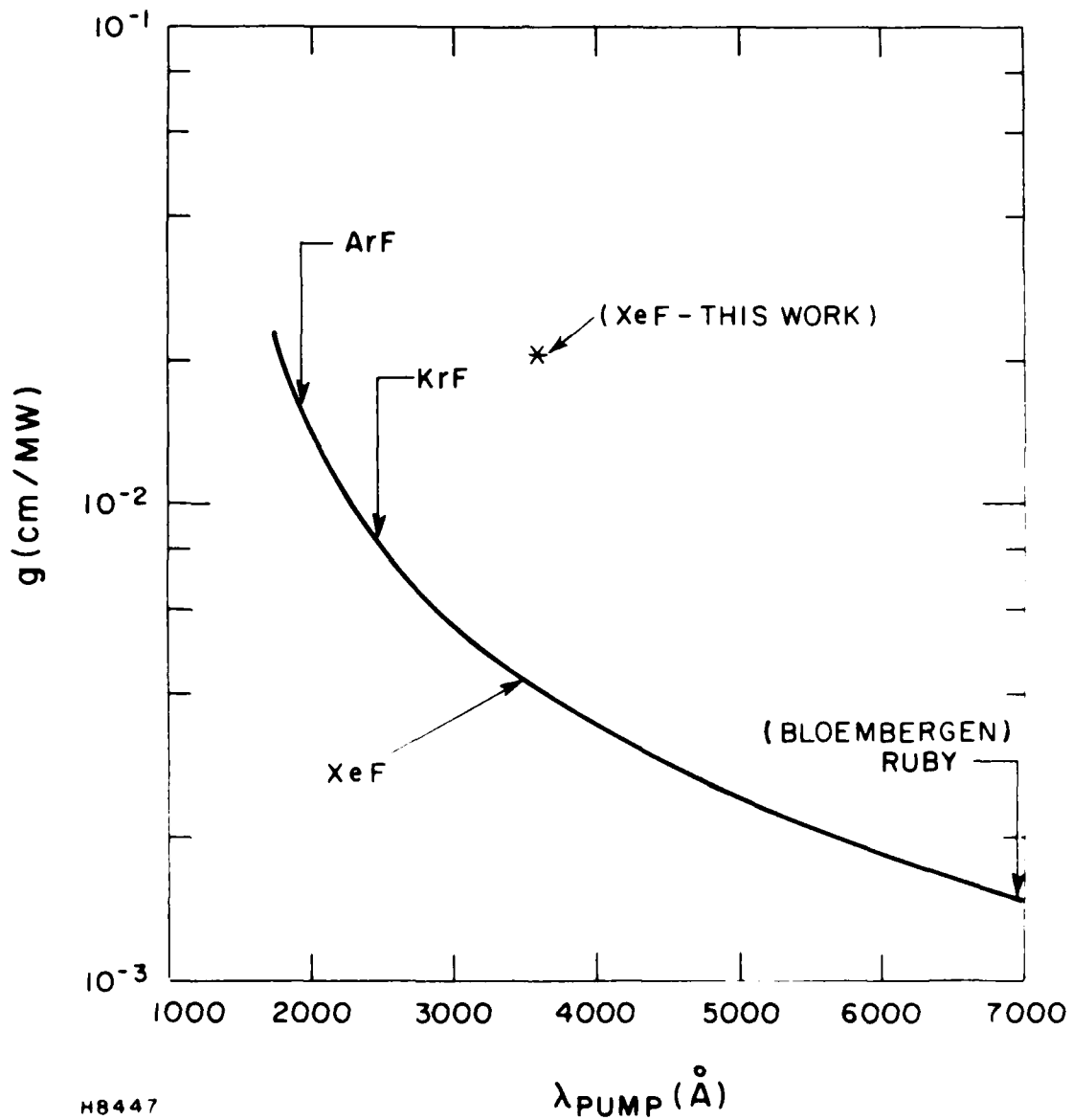
and $L = 8 \text{ cm}$

$$\therefore g = \frac{30}{I_{Th} L} = \frac{30}{1.9 \times 10^8 \times 8} = 2 \times 10^{-8} \text{ cm/W}$$

This value is about a factor of 5 larger than the value deduced from wavelength scaling of that reported by Bloembergen (Ref. 9) at Ruby wavelengths (see Figure 13). Since the theoretical wavelength scaling for the SRS cross section is fairly straightforward, our results suggest that Bloembergen's reported value may be too low. However, a more definitive gain measurement at the relevant wavelength ($\lambda \sim 350 \text{ nm}$) is required to resolve this apparent discrepancy.

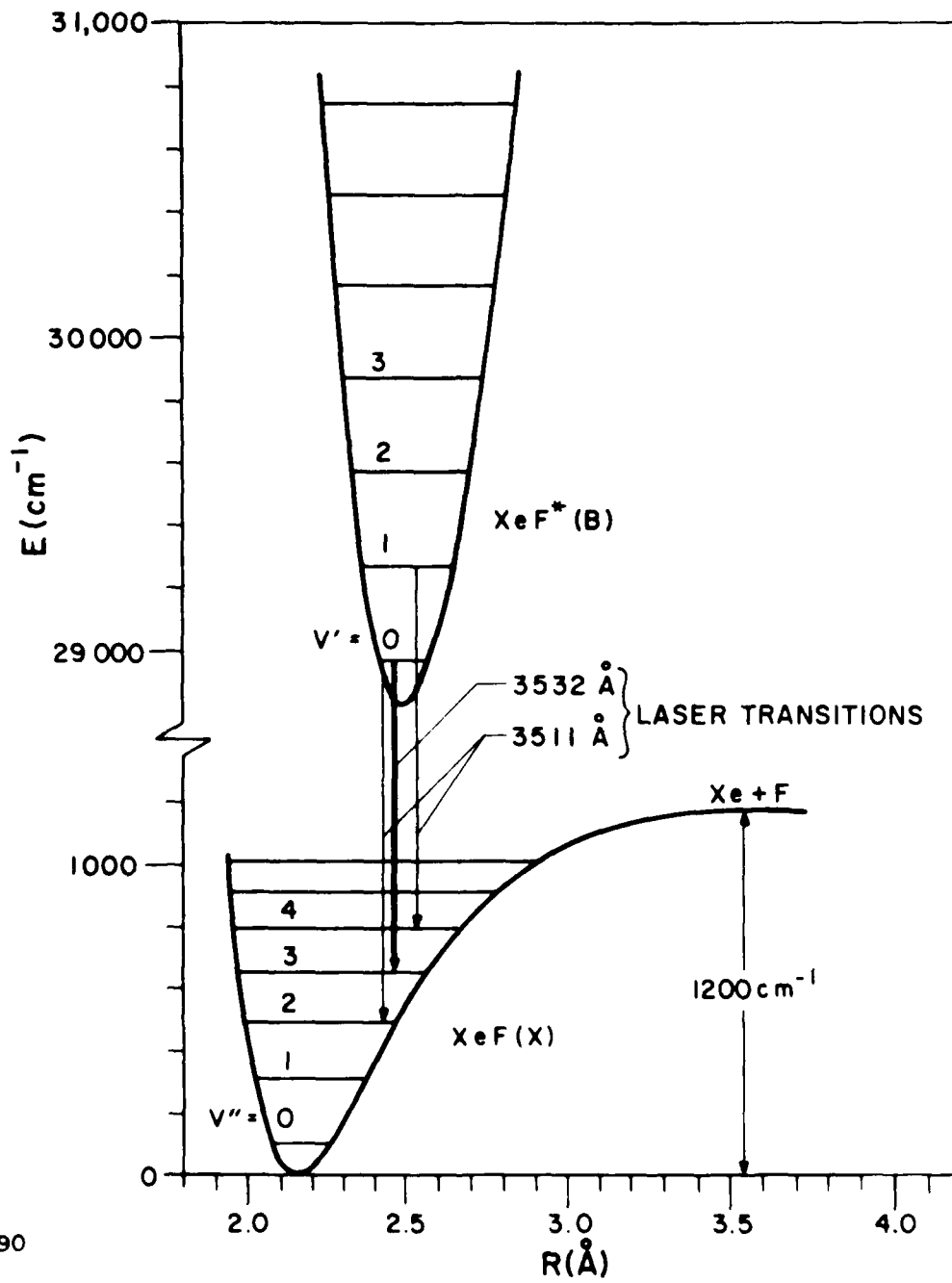
The pump laser produces output at both 3511 \AA and 3532 \AA (see Figure 14) with $\sim 80\%$ at 3511 \AA . The total temporal pulsewidth was measured to be 6 ns (FWHM). When these spectral lines were observed independently with a monochromator, their individual pulsewidths were still near 6 ns but the 353 nm line was delayed slightly from the 351 nm line. This observation is consistent with the observations of others of higher gain in the 351 nm band at room temperature (Ref. 10). Pulse shape measurements of the first Stokes pulses were initially performed with the experimental setup using the

10. Goldhar, J., Dickie, J., Bradley, L.P. and Pleasance, L.D., App. Phys. Lett. 31, 677 (1977).



HB447

Figure 13 First Stokes Gain for Forward SRS in H_2 . Solid line is wavelength-scaled calculation normalized to Bloembergen's result with ruby; * indicates the value deduced from this work.



H1990

Figure 14 XeF Lasing Transitions

50 cm focus (see Figure 9) at pressures of 10 atm. Characteristic pulse shapes are shown in Figure 15. The top traces show the input laser pulse with the 351, 353 nm XeF lines unresolved. The bottom traces are of the corresponding 411, 414 nm first Stokes lines. The temporal widths of these Stokes-shifted lines are ~4 ns. Similar effects were observed for the softer focus. Measurements of the pulse shape of the second Stokes component from a single cell did not show any further pulse distortion, i.e., they had essentially the same 4 ns pulsewidth as the first Stokes.

All of these data and the above discussion allow us to summarize the results of our single pass, single cell, XeF* pumped H₂ conversion efficiencies for optimized experimental conditions. Conversion efficiencies were calculated by measuring the output energy from the Raman cell through a series of spectral filters, then adjusting the recorded energy for the known transmission of the filters and finally ratioing it to that measured through an empty cell. A photon conversion efficiency of 100% is usually not achievable in these nonresonant molecular Raman systems because as the first Stokes radiation approaches high intensities, it itself acts as a pump and is converted to higher order Stokes emission. Table 1 contains a summary of the typical output and conversions observed. The power conversion efficiency is the relevant value, since the energy efficiency should

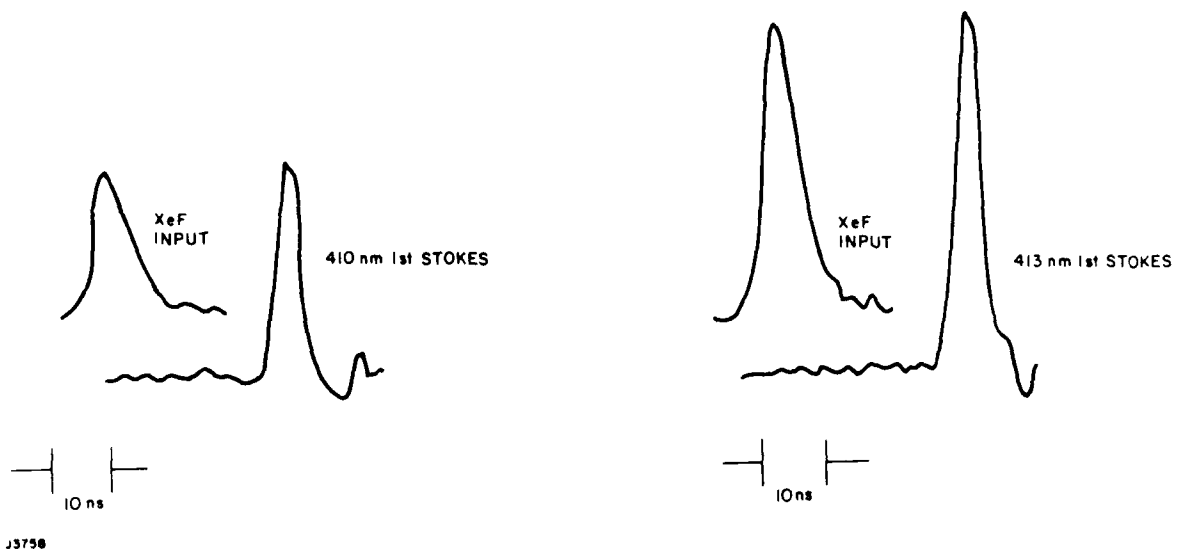


Figure 15 Temporal Characteristics of First Stokes (H_2) Spectral Lines Using the Short Focal Geometry

TABLE 1

SUMMARY OF SINGLE CELL XeF-PUMPED H₂ SRS CONVERSION EFFICIENCIES (Lumonics Experiments)

<u>Pump</u>	<u>Focus</u>	<u>E_{in} (mJ)</u>	<u>E_{out} (mJ)</u>	<u>Energy Eff (%)</u>	<u>Photon Eff</u>	<u>Power Eff</u>	<u>Power Photon Eff</u>
XeF	137 cm	9.6	4.2 S ₁	44	61	66	76

~0 S₂

approach the power efficiency for sufficiently long pulse-lengths. These reported efficiencies did vary somewhat from experiment to experiment, however, the values presented here were observed routinely. (The actual highest efficiency for conversion to S_1 with H_2 in a single experimental observation was 57% energy and 86% power conversion efficiency.)

Other stimulated Raman conversion efficiencies for H_2 reported in the literature include 20% photon efficiency into S_1 pumped by a 1.06 μ laser by A. Grasiuk (Ref. 11), while Komine and Stappaerts (Ref. 12), report power photon conversion efficiencies of near 50% into either S_1 or S_2 , when H_2 is pumped by a tripled Nd:Yag laser at 355 nm with an oscillator amplifier configuration. Loree, et al. (Ref. 8), have also reported up to 70% energy depletion into various Stokes orders for KrF pumped H_2 . All of these experiments suggest efficient conversion to longer wavelengths via stimulated Raman scattering in a single pass is readily achievable.

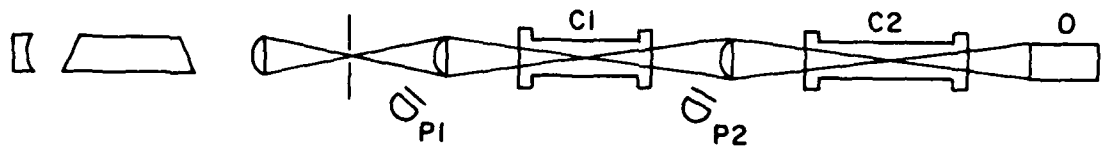
The next topic that we addressed in these short pulse, low energy experiments was the second step in the two-step process; namely, investigation of the conversion properties of the emerging S_1 from cell one, subsequently acting as a pump, to produce its S_1 in cell two. (see Figure 16).

The first of these experiments consisted of two-step shifting through two cells filled with hydrogen, i.e.,

11. Grasiuk, A., Private Communication (Dec. 1978).

12. Komine, H. and Stappaerts, E.A., Optics Lett. 4, 348 (1979).

2 CELL EXPERIMENTS



J3735

Figure 16 Schematic of Experimental Setup where C_1 and C_2 are the Two High-Pressure Cells and P_1 , P_2 the Photodiodes for Monitoring the Inputs to each Cell Respectively

XeF \rightarrow H₂ \rightarrow H₂. The first cell was optimized for maximum conversion of XeF* to first Stokes, S₁, at 411, 414 nm. These emerging laser photons were separated from the depleted pump via a dielectric coated mirror. The depleted XeF* pump was thus rejected, while the first Stokes beam from cell one was focused into the second cell, also optimized to convert into its own first Stokes at 496 and 500 nm.

Experimentally, the same conversion efficiencies observed through the first cell were not observed in the second step. This was essentially due to the limitations in S₁ energies (acting as the pump) which could be delivered into the second cell through the various optical components (mirror, lens, window, etc.). We were apparently just over threshold in pump laser intensity for the second-step SRS process.

Specifically, the XeF pump laser was focused into the first cell with a focal length of about 135 cm and the cell was maintained at pressures >40 atm to insure good conversion. The output light (depleted XeF* and S₁ radiation) resulting from this optimized configuration was collected and then refocused into a second cell. A dielectric coated mirror was usually employed, behind the first cell, to reflect > 99.9% of the depleted pump yet partially transmit (~50%) the first Stokes radiation. The waist diameter and conversion length of this S₁ radiation were

measured as before (see Figure 17). From this figure, the effective gain length is near 5 cm and the power density at the focus is estimated as follows:

0.05 cm pinhole

$$\frac{1.5 \times 10^{-3} \text{ J}}{4 \times 10^{-9} \text{ s}} \frac{4}{\pi (0.05)^2 \text{ cm}^2} = 1.9 \times 10^8 \frac{\text{W}}{\text{cm}^2}$$

0.04 cm pinhole

$$\frac{0.7 \times 10^{-3} \text{ J}}{4 \times 10^{-9} \text{ s}} \frac{4}{\pi (0.04)^2 \text{ cm}^2} = 1.4 \times 10^8 \frac{\text{W}}{\text{cm}^2}$$

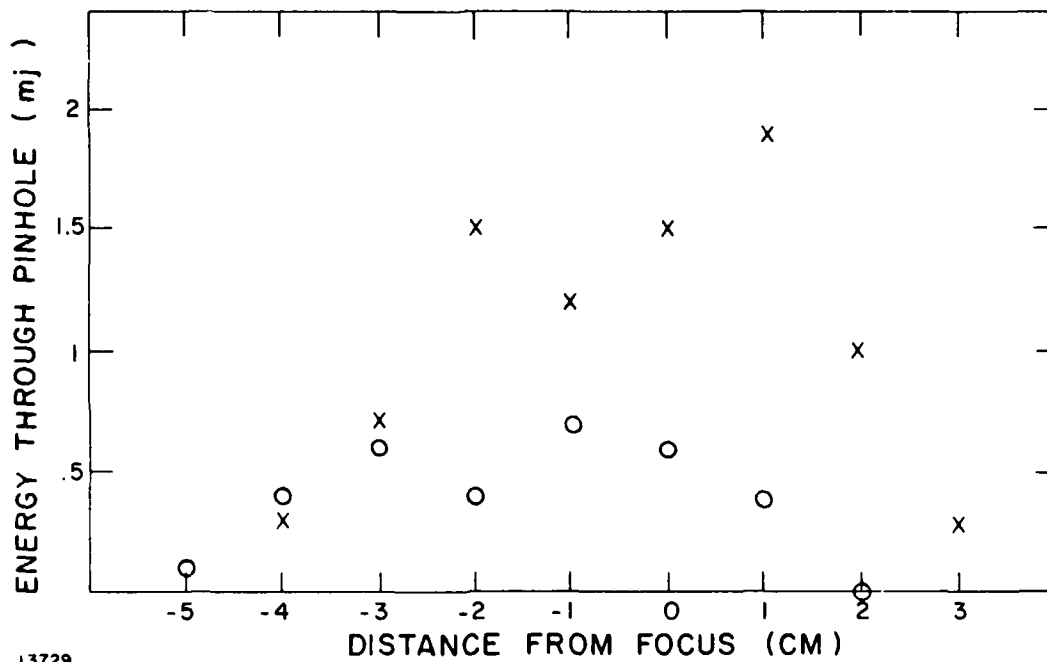
This represents a lower limit for the actual power density of this first Stokes laser light in that $\geq 50\%$ of the power was lost in transmission through the optical components. When these are taken into account, the measured power density of the first Stokes compares favorably with the XeF pump ($4.5 \times 10^8 \text{ W/cm}^2$) and indicates that the focusability of the emerging Raman Stokes shifted light is comparable to the pump.

The variation of the conversion features with the pressure in the second cell was qualitatively similar to that measured in the single cell experiments. Figure 18 shows a plot of the output as measured with the OMA when the pressure in the second cell was varied. (These data are not directly comparable in that the sensitivity of the OMA is greater at 500 nm than at 400 nm.) The points at "zero pressure" indicate that the input consisted of both S_1 and S_2 .

1st STOKES FOCUS AT CELL 2 - H₂

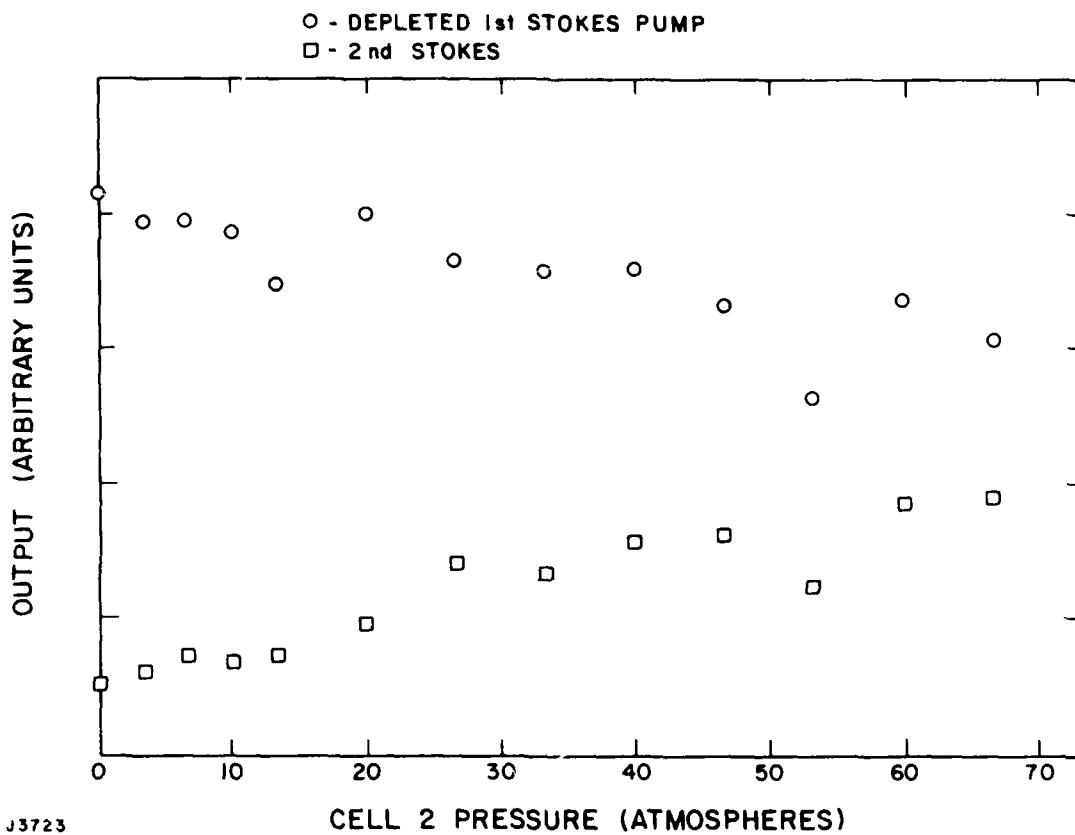
x - .05 CM DIA PINHOLE

o - .04 CM PINHOLE



J3729

Figure 17 Energy Measured Through 0.05 or 0.04 cm Diameter Pinholes vs Distance from Focus for S₁ Radiation



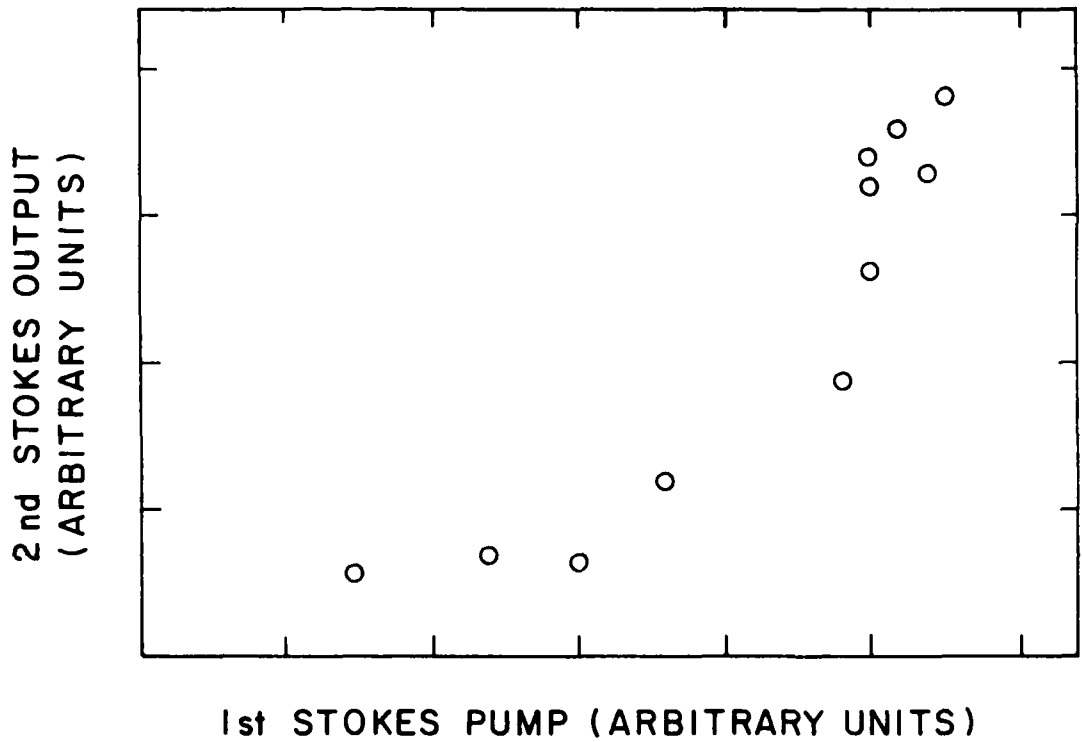
J3723

Figure 18 Cell 2 (H₂, H₂) Pressure Variation Effect on S₁ Pump and the Generation of S₂

Threshold in the second cell was measured by monitoring the first Stokes input with a photodiode and the second Stokes output with another photodiode. The results are summarized in Figure 19. In these experiments, the first Stokes, acting as a pump in the second cell, is probably not far above threshold.

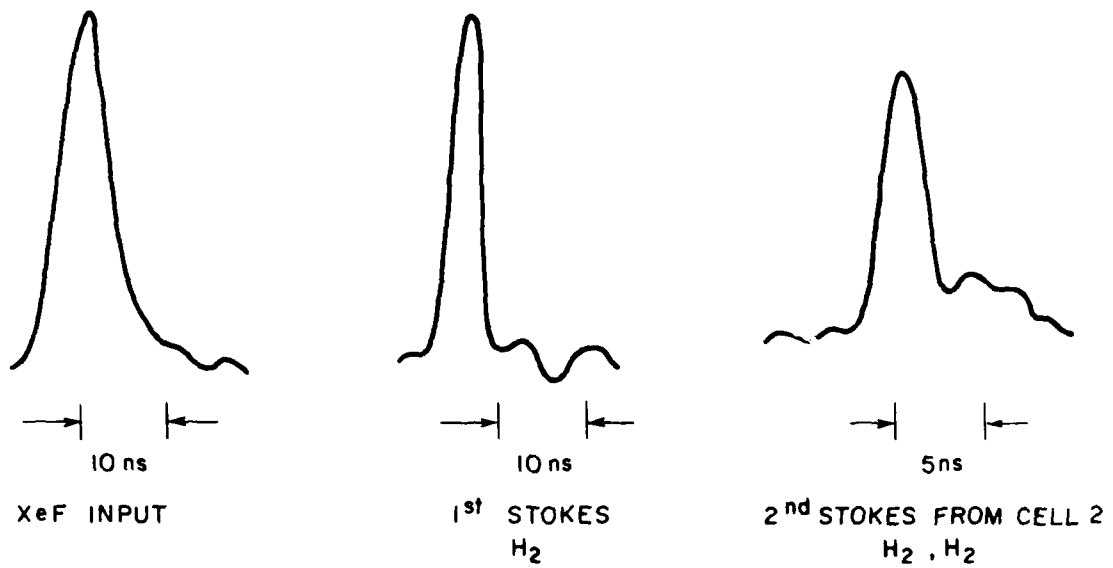
The intensity-length product for conversion of $\text{XeF}^*/\text{H}_2/\text{H}_2$ can be calculated from these second-cell experiments. The threshold energy was near 1 mJ. The pulselength was 4 ns with a beam waist of 0.05 cm and a conversion length ~5 cm at the focus of the second cell. The intensity-length product is, therefore, near 6×10^8 W/cm which is considerably less (even after wavelength scaling is accounted for in the calculation) than the value calculated from the single-cell experiments. This lowered (apparent) threshold is caused by the presence of a small amount of second Stokes radiation emitted from cell 1 and entering into cell 2. This small amount of second Stokes can act as the initial input for the conversion process and would require less amplification (i.e., a total gain significantly < 30) for stimulated Raman scattering to occur.

The temporal features of the two-step conversion are depicted in Figure 20. This figure shows the XeF pump, the first Stokes output of cell 1 and the second Stokes output of cell 2, when both cells were filled with H_2 .



J3724

Figure 19 Cell 2 Threshold for S_2 as a Function of S_1 Input Intensity



J3749

Figure 20 Pulse Temporal Narrowing in Successive Conversion

The pulsewidth goes from 6 ns for the XeF laser to 4 ns for S_1 to 2.5 ns (FWHM) for S_2 , although the general pulse shapes remained the same.

The typical energy conversion efficiency measured in this manner was 25 to 30% into S_2 output from the S_1 input, i.e., 496 out/411 in. This corresponds to a photon conversion efficiency of 30 to 35%, a power efficiency due to pulse shortening of 40 to 48% and a photon power efficiency of 48 to 56%. The total power conversion efficiency from the XeF input into cell 1 into S_2 output from cell 2 was 29%. As discussed above, conversion efficiency characteristics of what was achieved in a single cell should be achievable in any subsequent cell for an overall conversion of $\eta_1\eta_2$. Since we measured power conversion efficiencies of 66% in a single cell, overall conversion $>40\%$ to the blue-green should be achievable, but were unobtainable here due to the low pump intensities available.

This conjecture was tested somewhat by conducting two-step experiments with KrF* as the pump. The KrF laser operates at higher output intensities and was capable of generating significant quantities of S_1 through D_2 (see Figure 21). In this case, the first cell contained 67 atm of D_2 which resulted in an output consisting mainly of depleted pump (249 nm) and S_1 at 268 nm. These laser transitions were collected and focused into the second cell

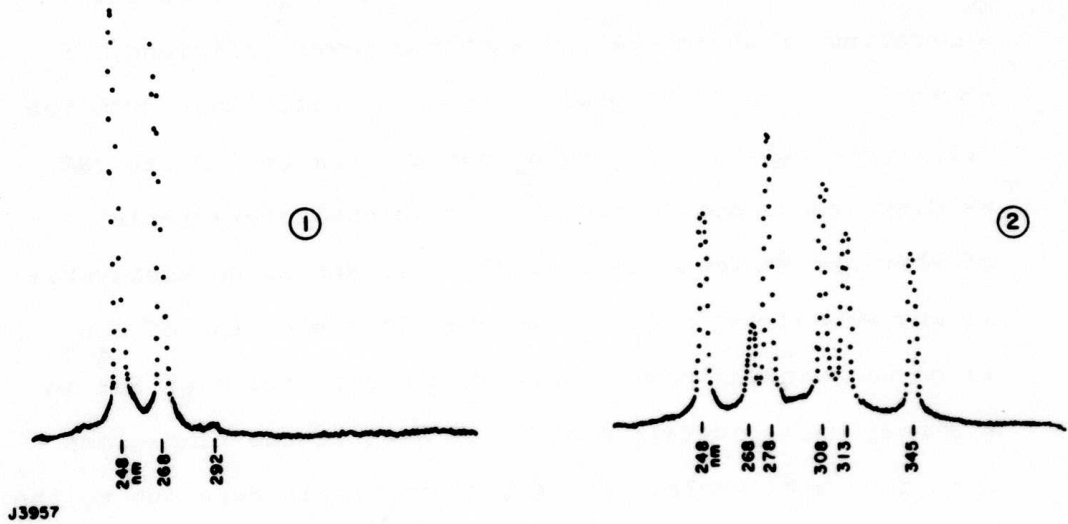
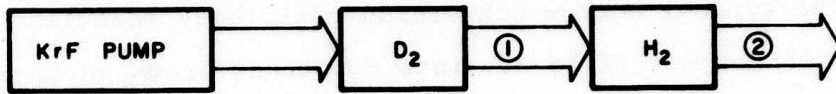


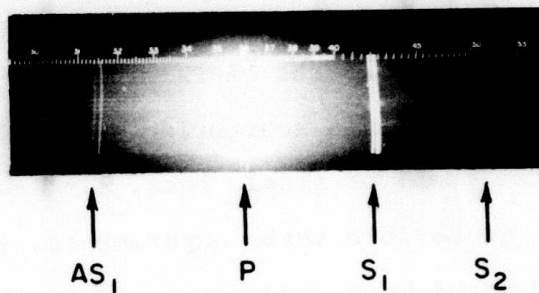
Figure 21 Two-Step KrF/D₂/H₂ Raman Conversion

containing H_2 . They each generated their own Stokes components in cell 2, but most of the output consisted of a few first Stokes orders (see Figure 21). Of particular interest is the fact that the 268 nm S_1 output of cell 1 was depleted over 70% in cell 2, with the majority of the output appearing in the sought after 308 nm line (which would be analogous to the production of 470 nm with XeF as the pump).

2. Long-Pulse Laser Experiments: 1-Meter E-beam Pumped Lasers

Included as part of the DARPA-supported program, we also investigated Raman scattering using the output of a 1 m laser as the pump for single pass, single cell spectral observations. To perform these experiments, two different e-beam laser devices were used. The first experiments, which were carried out in FY '79, involved the (10 x 10 x 100) cm^3 device. It was run with conventional optics and provided ~5 J in 600 ns for the few experiments we tried. Under these conditions, the output was collected by a 6-inch Dynasil UV-1000 quartz plano-convex lens (50 cm fl) and focused into the center of our high-pressure H_2 cell (~10 atm). We observed output spectra corresponding to S_1 , S_2 and AS_1 (see Figure 22). From color Polaroid open-shutter photographs, it appeared that the output consisted of principally parametric four-wave conversion processes as was evidenced by the observation of annular rings (see Ref. 6). Also, the intensity

LONG PULSE LENGTH XeF* SRS EXPERIMENT
(10 ATM H₂)

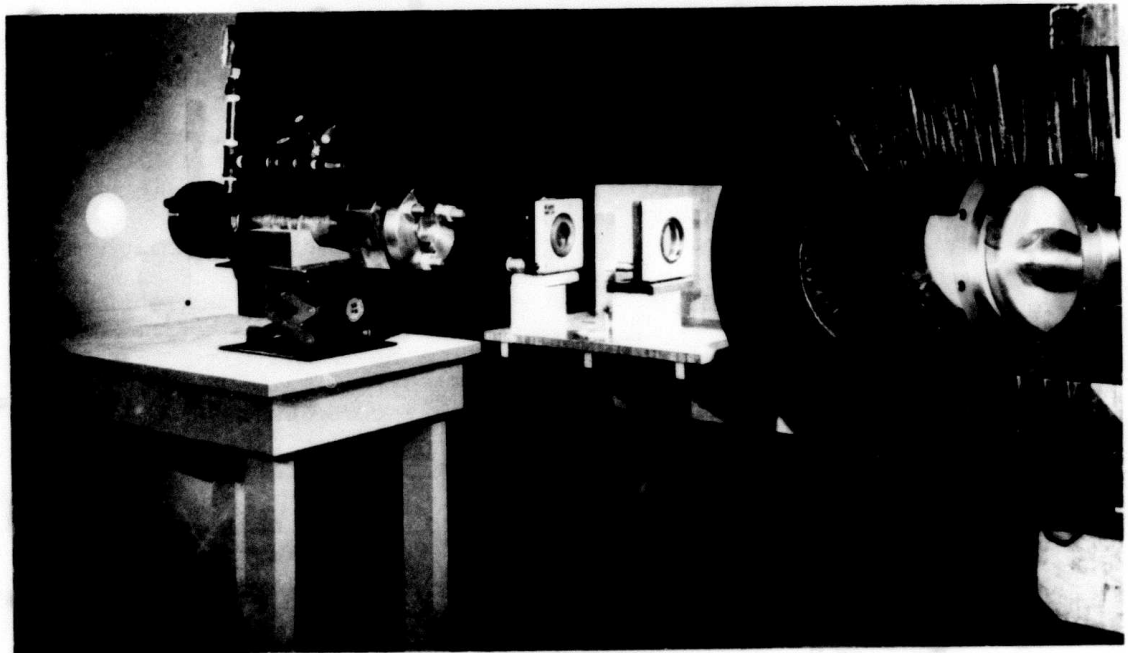


J3827

Figure 22 Spectra Giving Qualitative Indication of Relative Intensities of XeF Pumped H₂ (AS₁, P, S₁, S₂)

correlations in the Stokes radiation ($AS_1 > S_2$) supported this contention.

More recently, we have been performing stimulated Raman scattering experiments using another 1 m long, e-beam initiated XeF laser as a pump. The e-beam was a high energy (400 kV) Marx bank driven device (Systems, Science and Software, model 450) operated at current densities near 18 A/cm^2 . The electrons entered the laser cavity through a $100 \times 4 \text{ cm}$, 1 mil Kapton foil, with two external magnets providing a guide field to confine the beam and give uniform deposition into the gas. The laser mix consisted of 0.1% NF_3 , 0.5% Xe and the balance Ne, at a total pressure of 60 psi. The active laser cavity was fitted with Dynasil UV-1000 quartz windows set at the Brewster angle. Several cavities were tried. Initial experiments, similar to those performed using the 10 cm aperture device, used a conventional flat-flat resonator; the resulting output was focused into the center of a small H_2 Raman cell and significant conversion to the blue-green was observed (see Figure 23). Later experiments utilized a positive branch confocal unstable resonator with a magnification of 2.35. The two aluminum coated front surface cavity mirrors, with a nominal reflectivity of 92% at 353 nm, were spaced 267 cm apart. The output coupler was an aluminum scraper mirror set at 45° , which produced a square exit beam with a $4 \times 4 \text{ cm}$ outer



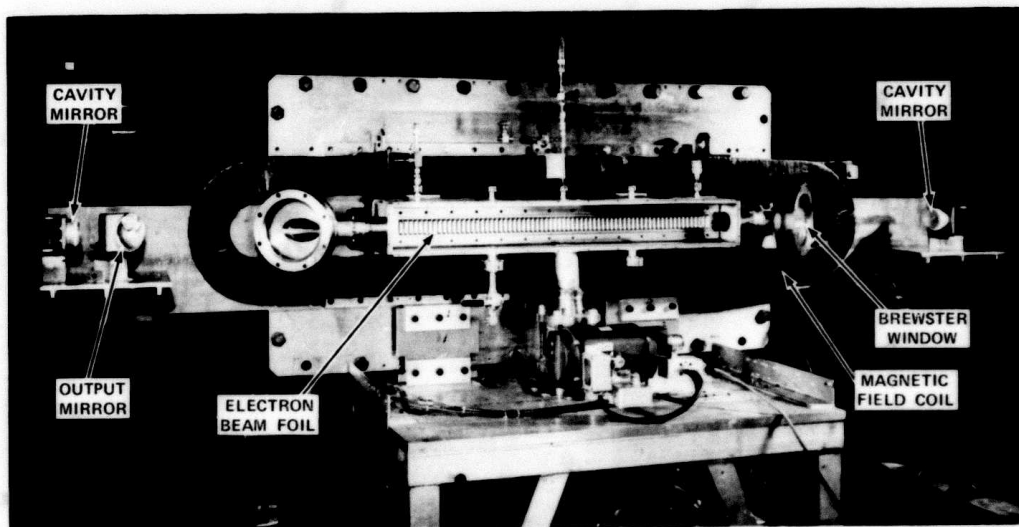
J9096

Figure 23 Blue-Green Optical Conversion of XeF* (1 Meter Device)

dimension and a centered obscuration (see Figure 24). Typical output energy was ~ 1 J in 0.4 μ sec. Measurements of energy through a pinhole indicated focused (50 cm focal length plano-convex lens) intensities ≥ 0.7 GW/cm². This output beam was of sufficient quality that it could be collected by various focal length lens and focused into the center of hydrogen Raman cells of varying overall lengths (the cell lengths were varied to reduce the fluence incident on the input windows). In this way, significant generation of a variety of Stokes shifted radiation could be produced (see Figure 25).

In these initial experiments, it was our objective to convert the output of this long pulse length XeF laser efficiently to stimulated Raman output. To perform these experiments and provide insight into the underlying physics operable under our conditions, the following experimental parameters were varied to explore the Raman process: focal length, pressure, and pump intensity (see Figure 26).

ation in the focal length, since intensity \times length is a constant, is expected to provide a changing distribution of angles which could influence the phase matching conditions for four-wave processes. With regard to the desired Raman process, provided the depth of field at the focus is small compared to the cell length, there should be no impact.



J3829

Figure 24 Photograph of 1-m Xenon Fluoride Laser

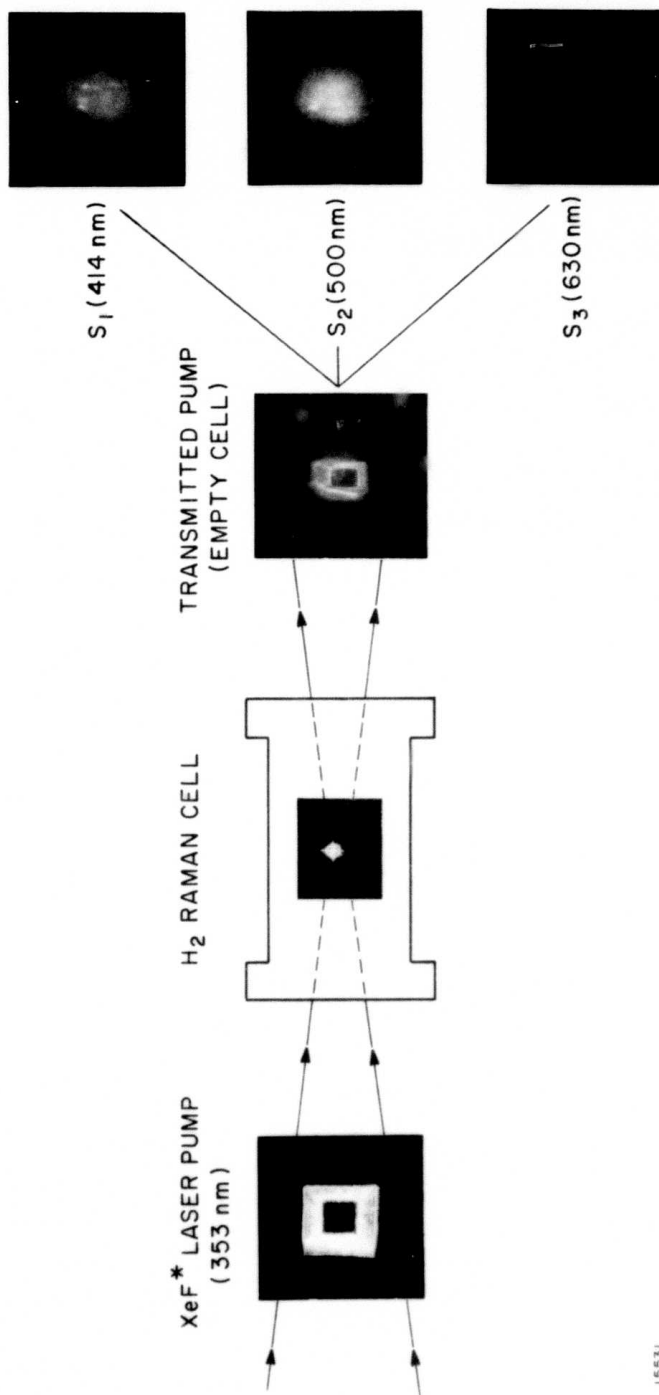
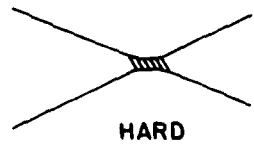


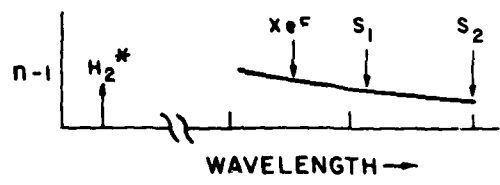
Figure 25 Stimulated Raman Output from XeF Pumped H₂

J5531

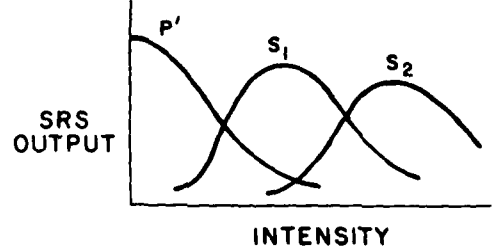
FOCAL LENGTH (IL = CONSTANT)



PRESSURE (g ~ CONSTANT)
⇒ AFFECTS DISPERSION



PUMP INTENSITY



J7003

Figure 26 Experimental Parameters Used to Explore Raman Process

Similarly, since at our operating pressures, the Raman gain is constant and independent of pressure, variations in pressure are expected to affect dispersion, although very insensitively due to the nonresonant wavelength regions involved. Again, the expectation is to vary the ability of various parametric processes to phase match and, therefore, alter the output observed.

Lastly, and most significantly, are variations in XeF pump intensity to observe threshold behavior of the various Stokes shifted radiation:

$$I_S(L) = I_S(0) e^{g_S I_P L}$$

The Raman gain is given by:

$$g_S = \frac{\lambda_S^2}{h\nu_S} \frac{N}{\pi \Delta\nu_R} \frac{\partial\sigma}{\partial\Omega}$$

where λ_S is the Stokes wavelength in the medium, N is the number density of molecules, $\frac{\partial\sigma}{\partial\Omega}$ is the spontaneous Raman scattering cross section and $\Delta\nu_R$ is the full width at half maximum of the Raman linewidth in H_2 . A plot of first Stokes gain versus wavelength is provided in Figure 27.

For the case of stimulated Raman scattering building from the initial spontaneous noise, a total gain of ~ 30 is required. This suggests that sequential Raman processes, i.e., I_p providing S_1 ; I_{S_1} producing S_2 , etc., involves a very large total gain length. Parametric generation of higher order Stokes radiation, not being a gain

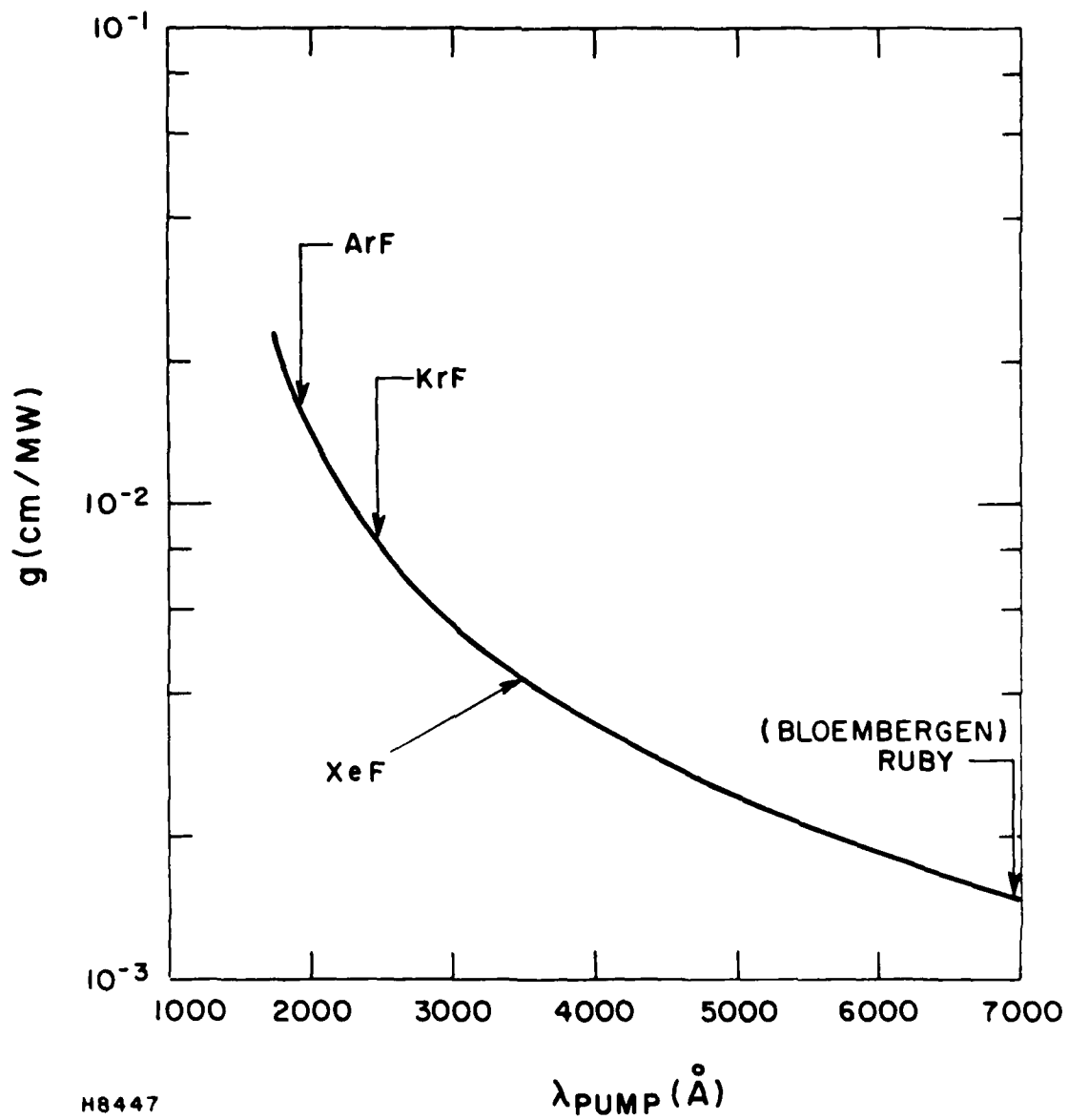
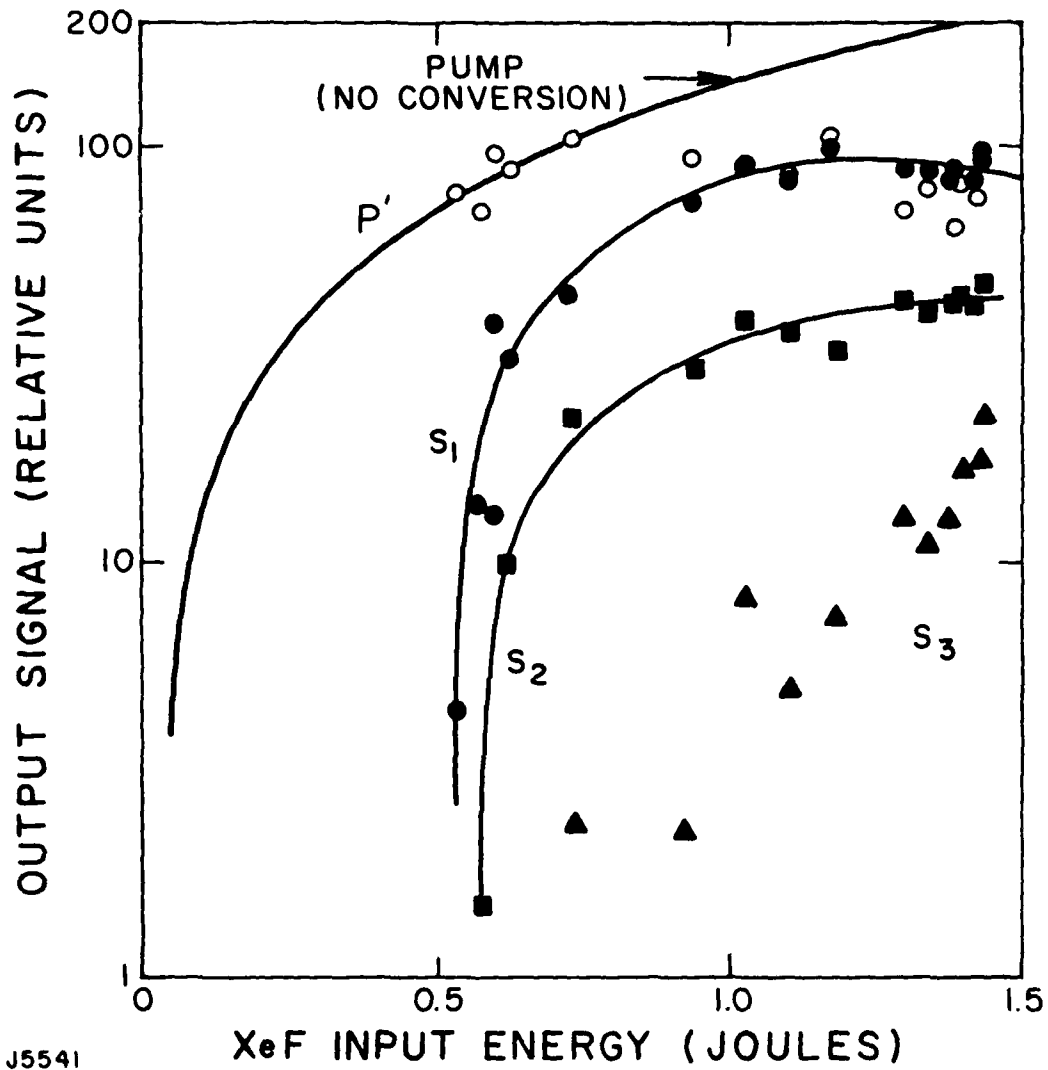


Figure 27 First Stokes Gain for Forward SRS in H_2

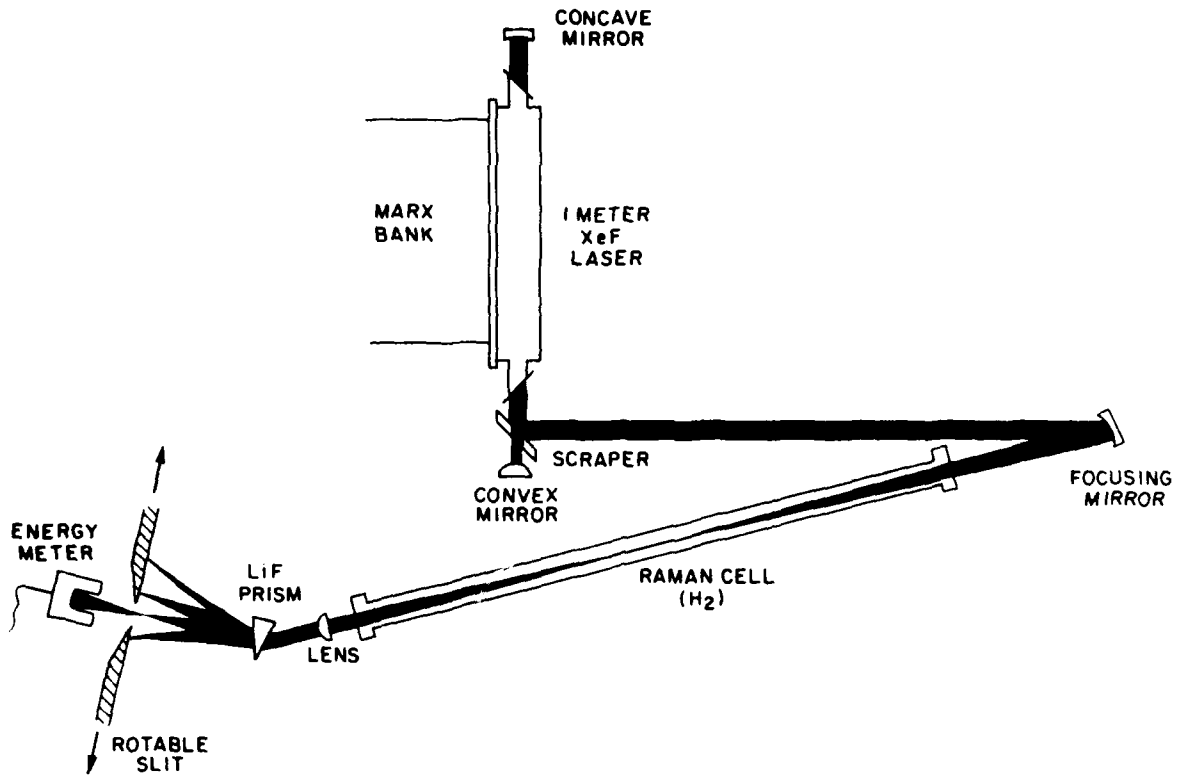
process, however, can be quite easily initiated, e.g., see Figure 28. From the data in this figure, it is readily seen that at threshold levels for the generation of S_1 at 414 nm, S_2 at 500 nm and S_3 at 624 nm are simultaneously present. This is very strong evidence for the presence (at high conversion efficiency) of parametric processes. These data were taken at 26 atm and used a hard focal length experimental setup (1.35 m). The interpretation of these parametric processes and their continued interplay and influence on the observed stimulated Raman output were a central thrust of our experimental program.

To perform these experiments, several techniques to vary the focal length were used. One (depicted in Figure 29) was to utilize a focusing mirror; the other technique involved varying the focus by the relative position of two lenses, then turning the corner with a flat 100% reflector. Both techniques gave essentially the same Raman results, although the lens/flat arrangement minimized astigmatism. By passing the output of the Raman cell through a LiF prism, the beam was dispersed into spatially resolved individual beams so that each could be sampled (in separate experiments) by an energy meter. The results for a typical set of experiments are summarized in Table 2. Here data are presented for two pressures: 7 and 70 atm. The distribution of measured radiation as energy percent as well



J5541

Figure 28 SRS Threshold Data (1.35 m focus: 26 atm H₂)



J6444

Figure 29 Energy Conversion Measurement Experimental Setup

TABLE 2
 CONVERSION EFFICIENCIES MEASURED FOR XeF* PUMPED H₂
 (1-m Device Experiments)

	<u>ENERGY (PHOTON) %</u>		<u>ENERGY (PHOTON) %</u>	
	7 AMG		70 AMG	
PUMP	51	(51)	54	(54)
S ₁	26	(30)	31	(36)
S ₂	14	(20)	6	(8)
S ₃	~ 1	(1.6)	~ 1	(1.3)
AS ₁	~ 2	(1.8)	~ 1	(1)
	<hr/>		<hr/>	
TOTAL	94%	(~ 104%)	93%	(~ 100%)

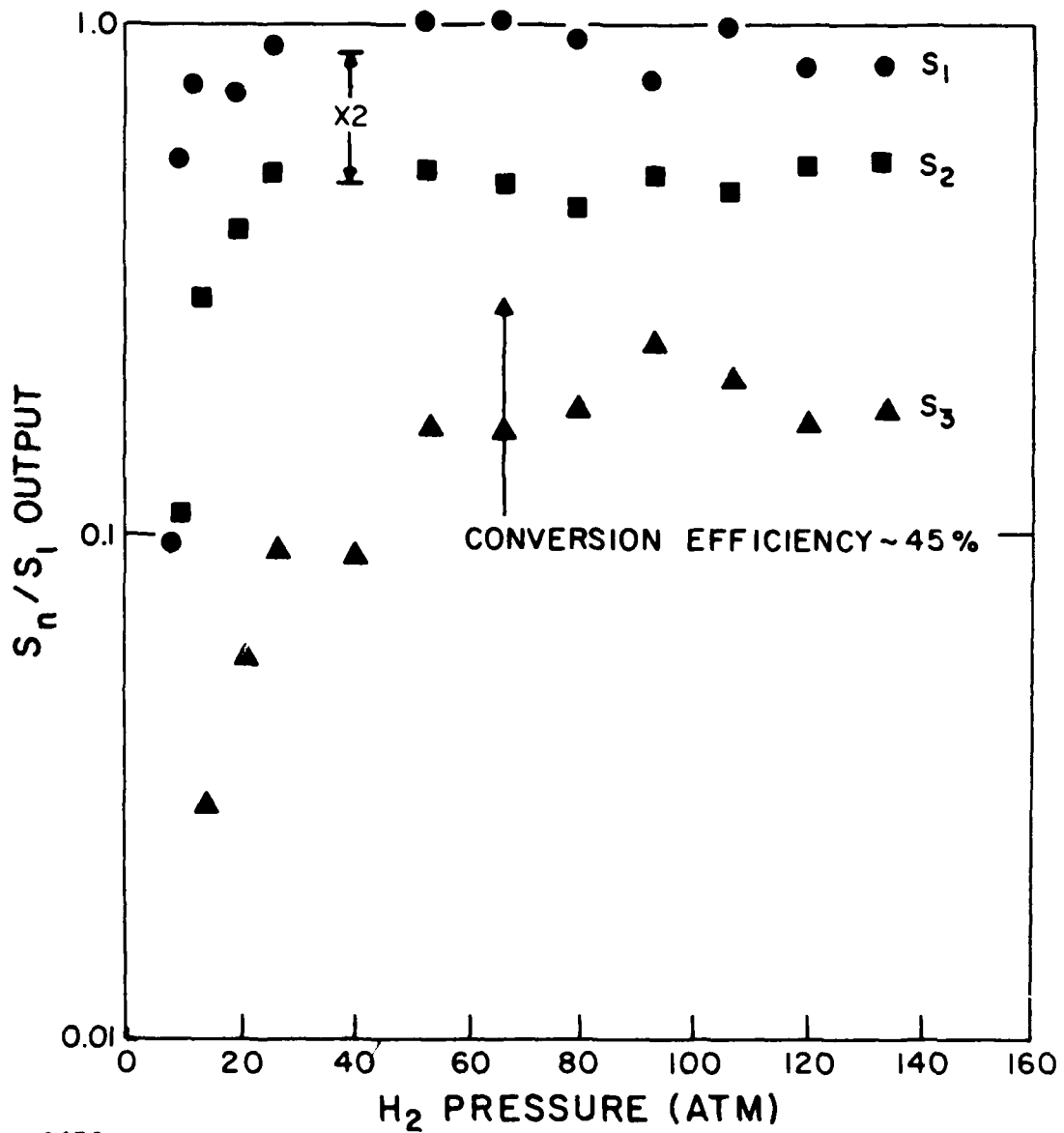
J6442

as photon conversion is shown. This type of energy book-keeping allowed us to calibrate the optical multichannel analyzer (Tracor Northern) and use it as a secondary standard allowing for a much more rapid data collection and reduction rate.

Typical data for various focal lengths as a function of pressure are shown in Figures 30 through 33. The data from the 1.35 m focus and the 3.6 m focus show evidence for significant effects from parametric processes (e.g., S_3 magnitude). A check on the 3.6 m interpretation is found in Figure 34 where simultaneous thresholds are observed as before.

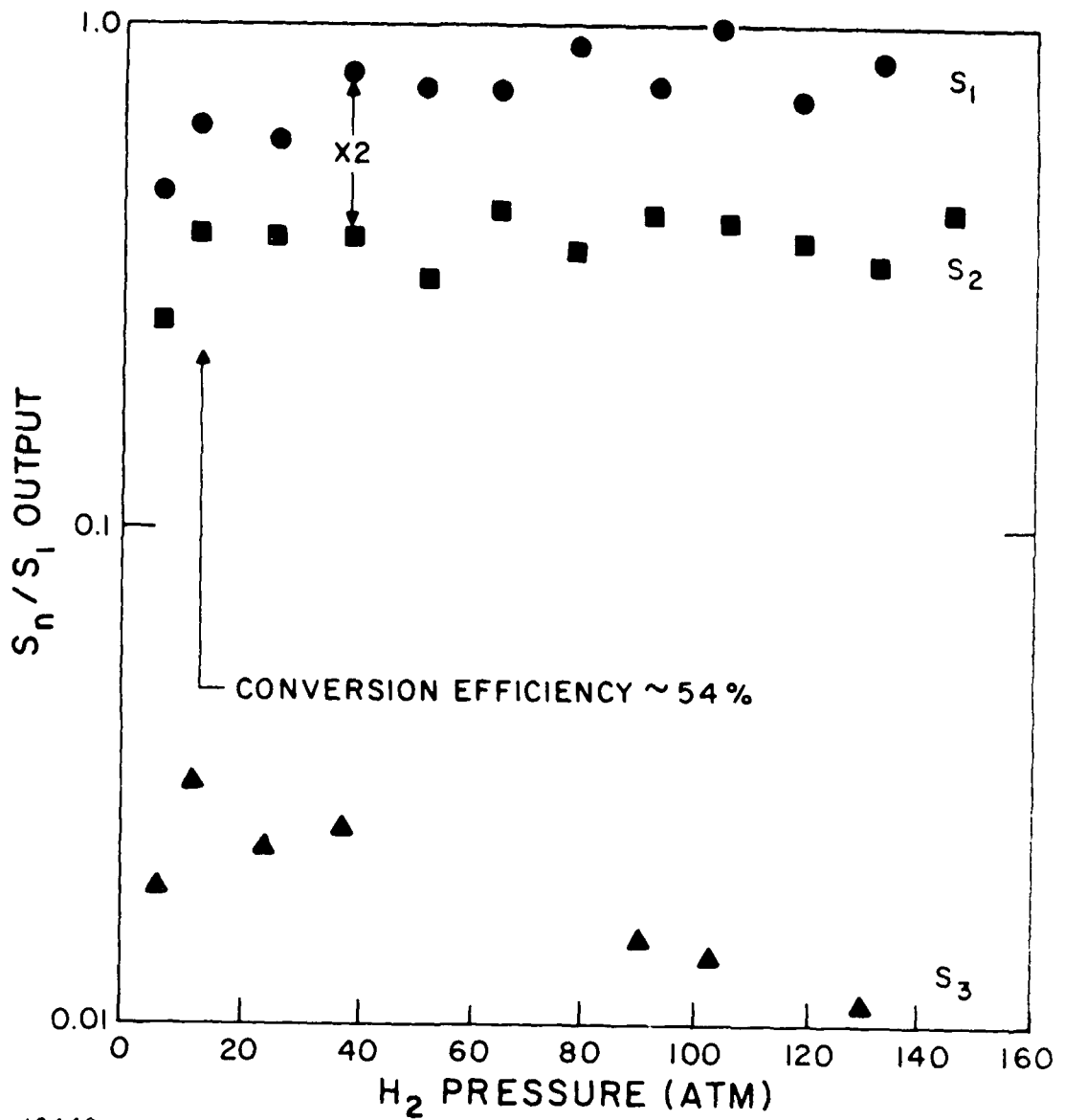
At the softer focus (4.6 m and 5.1 m), suppression and virtual elimination of S_3 was observed as well as enhanced conversion efficiency (see Figures 35 and 36). These data were recorded using spectrally filtered photodiodes which monitored the XeF input and output as well as S_1 and S_2 radiation. High depletion of the XeF pump ($> 70\%$) was observed both by integrating the area under these traces as well as by using the OMA. This increase in pump depletion is consistent with a decrease in parametric processes which may, for example, regenerate the pump (e.g., $S_1 + S_1 \rightarrow S_2 + P$).

The threshold behavior (Figure 37) at the softest focus investigated (5.1 m - essentially limited by room dimensions) shows distinct, different thresholds for



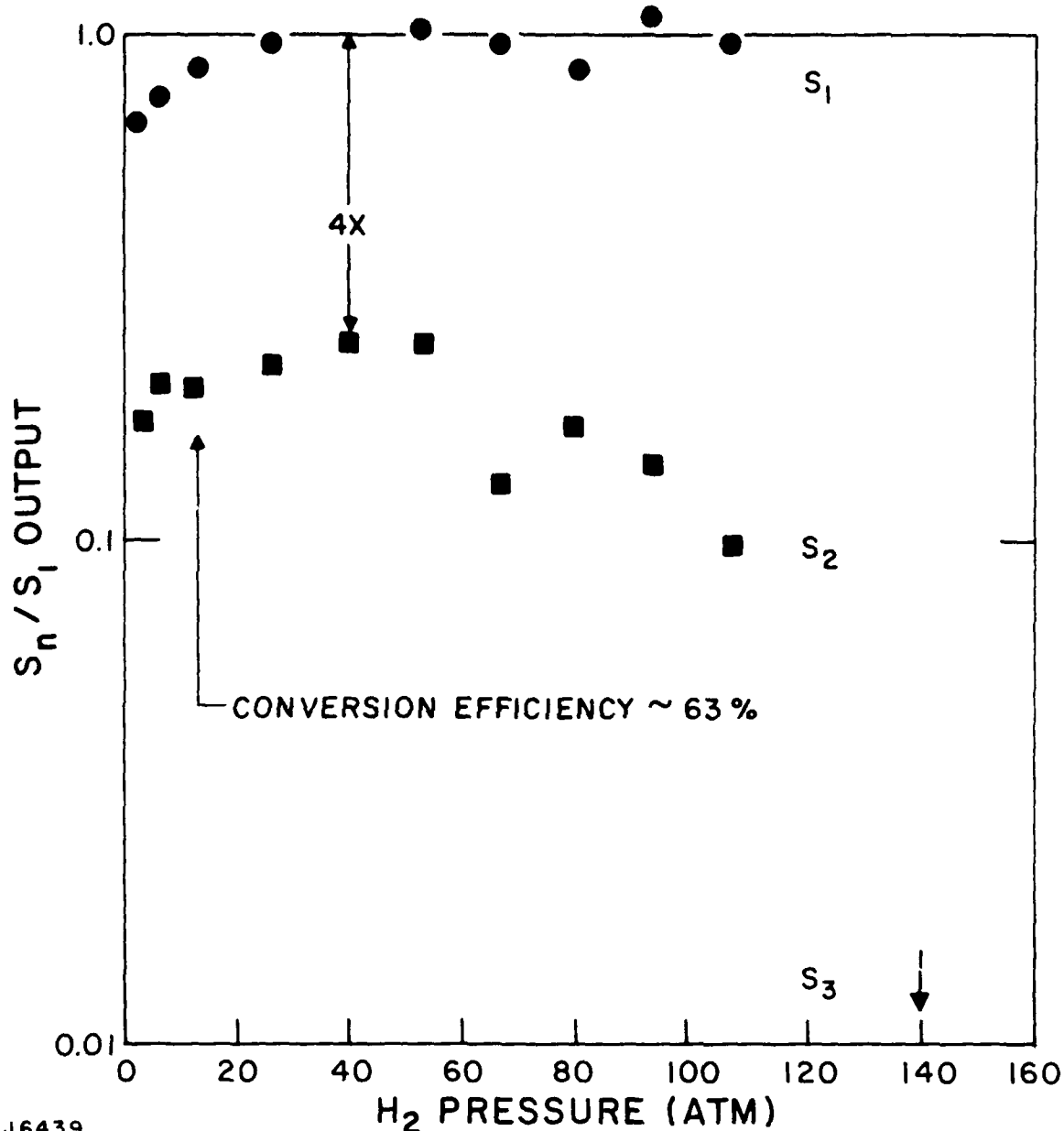
J6438

Figure 30 Significant S₃ Production at Hard Focus (1.35 m)
 Plot of S_n/S₁ vs H₂ Pressure



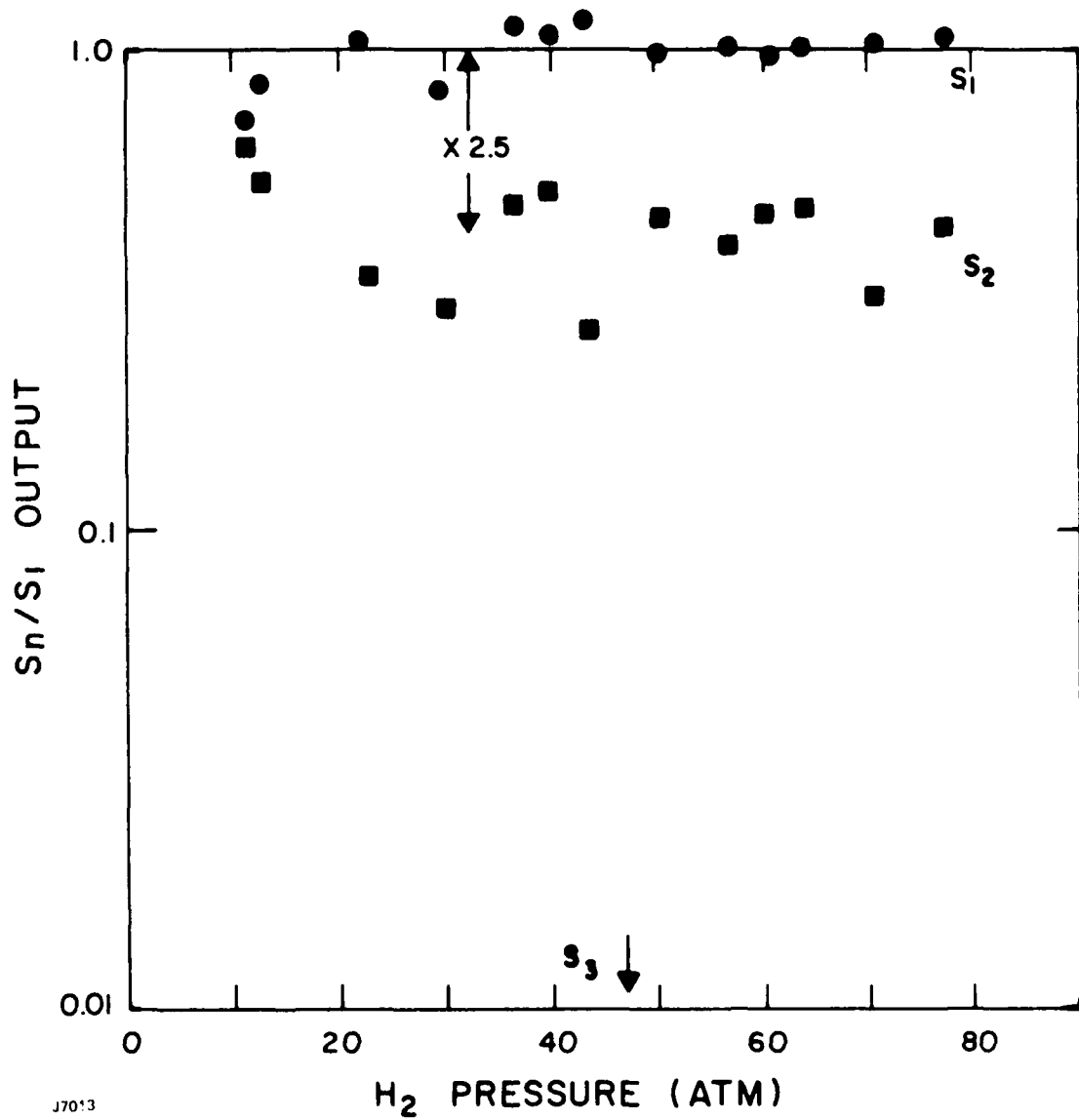
J6440

Figure 31 Reduced S₃ Production at Softer Focus (3.6 m) Plot of S_n/S₁ vs H₂ Pressure



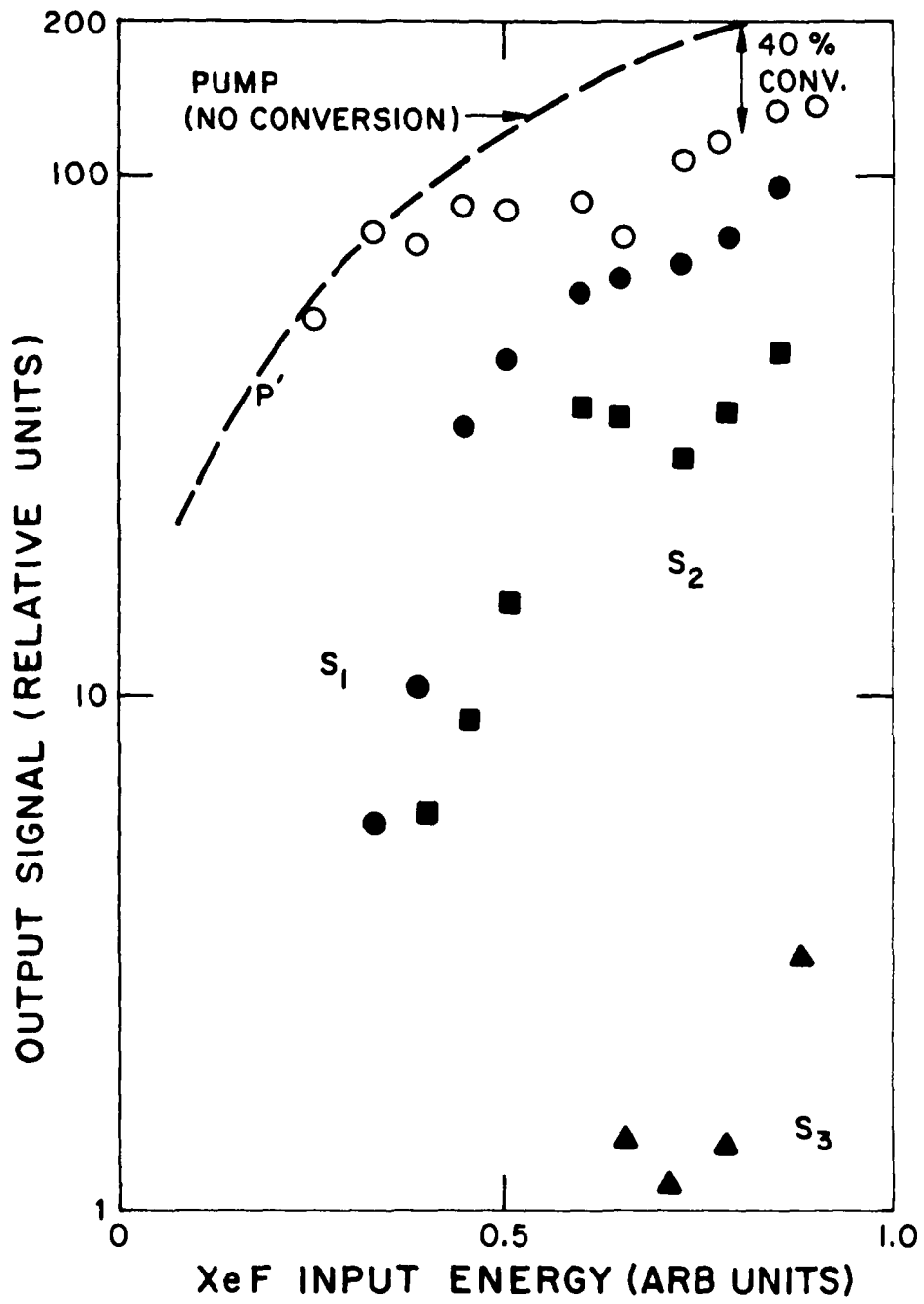
J6439

Figure 32 S_1 Dominates at Soft Focus (4.6 m) Plot of S_n/S_1 vs H_2 Pressure



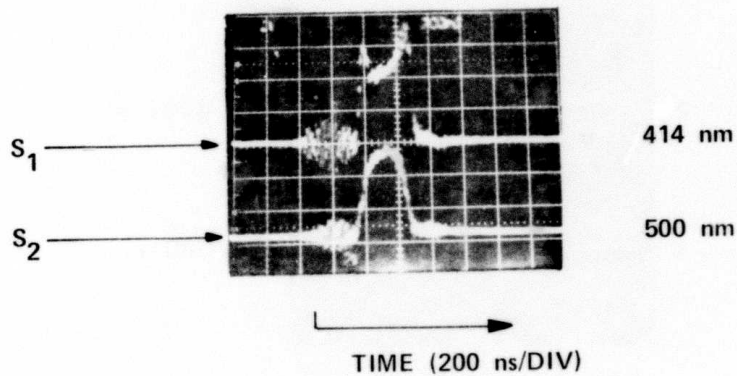
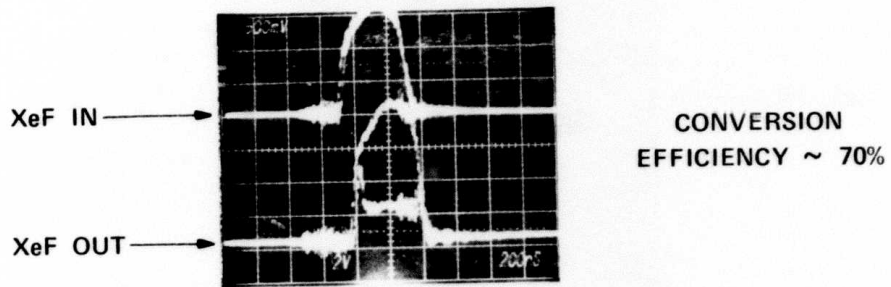
J7013

Figure 33 Pressure Insensitive S_1 and S_2 Output at Softest Focus Studied (5.1 m), Plot of S_n/S_1 vs H_2 Pressure



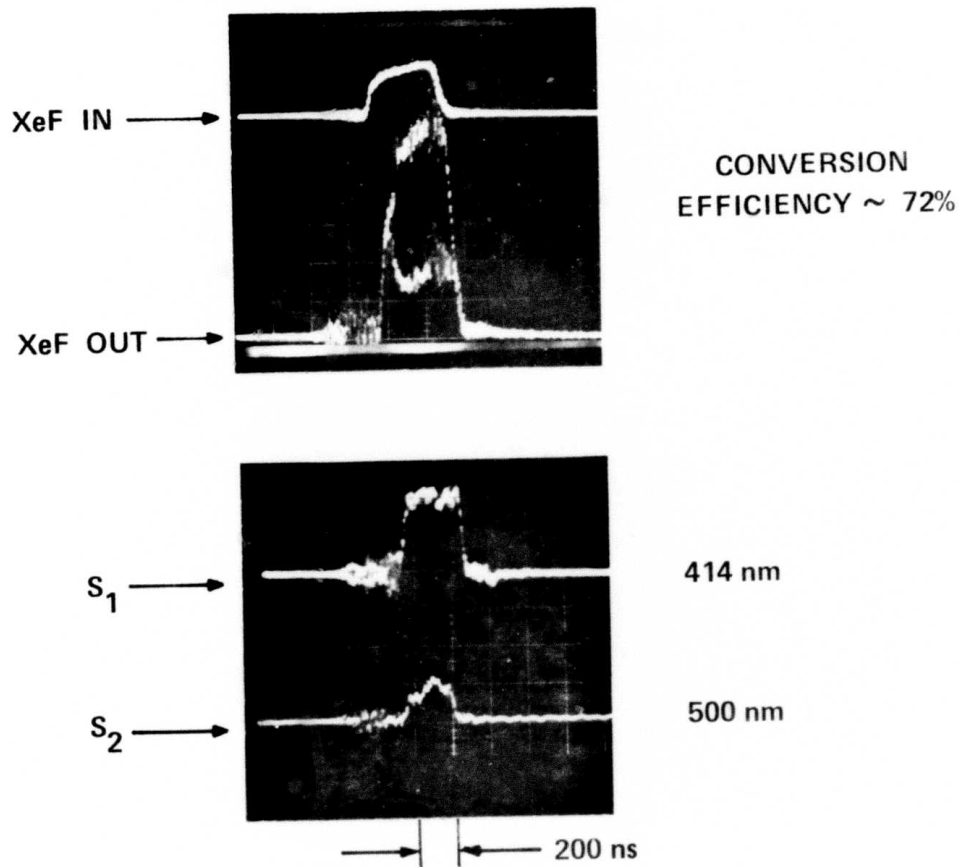
J6441

Figure 34 SRS Threshold Behavior (3.6 m focus)



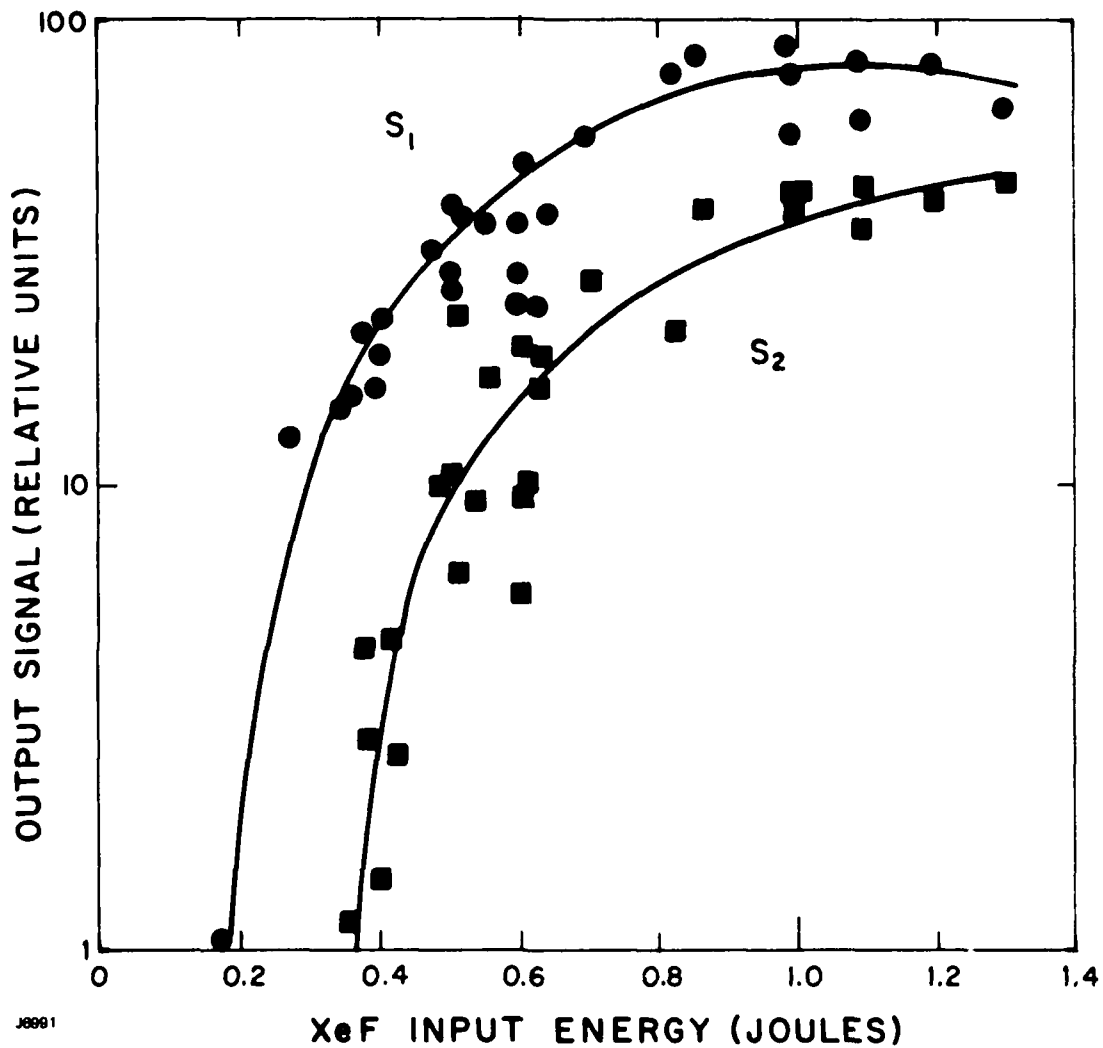
J6445

Figure 35 Raman Temporal Signals Observed at Soft Focus (4.6 m) Showing Pump Depletion of 70%



J6989

Figure 36 Raman Temporal Signals Observed at Softest Focus Studied (5.1 m) Showing Pump Depletion of 72%

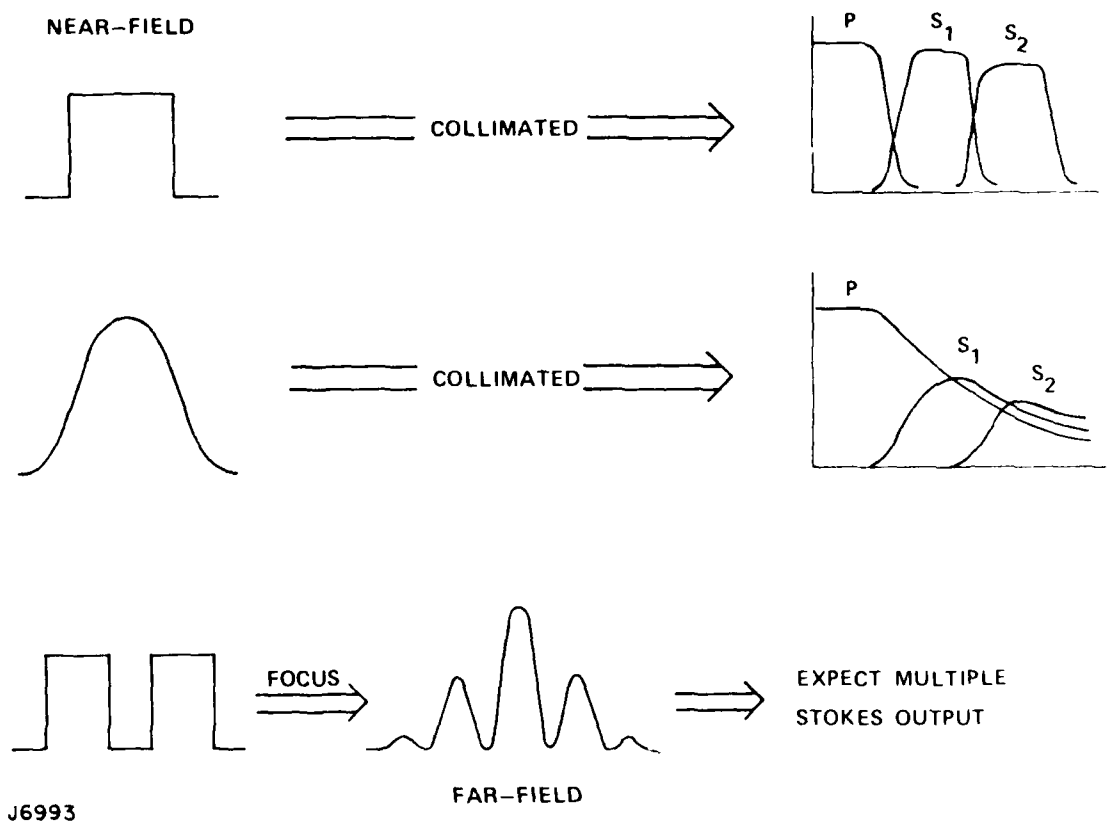


J8991

Figure 37 Different Thresholds Observed for S₁ and S₂ at 5.1 m Focal Arrangements

S_1 and S_2 and an indication that S_1 might be decreasing at the highest pump energies studied (~1.3 J). To properly interpret these results, a thorough knowledge of the spatial properties of the pump beam is required; since the nature of the spatial beam profile impacts the Raman result (see Figure 38). Most modeling has considered only collimated beams with either "flat top" or Gaussian spatial profiles in the near field. Our unstable resonator is expected to produce a "near flat top" profile (depending on its beam quality) and focus to a pattern similar to that shown at the bottom of Figure 38. With such a beam, multiple Stokes output is expected due to sequential conversion in those portions of the beam at highest intensities, just threshold S_1 production for the less intense portions, and no conversion at all for the smallest lobes.

To improve the conversion depicted by the data presented in Figure 37, we improved our cavity optics (including use of dielectric coated 100% reflectors) and alignment procedures; this allowed us to achieve higher W/cm^2 due to improved beam quality as manifested by a reduction in energy threshold and alteration in the S_2 to S_1 ratio (see Table 3). After laser beam quality improvements, increased S_2 production was observed at similar overall conversion efficiency. These data suggest near complete conversion of the depleted XeF radiation to Raman output; further improvements in conversion efficiency is limited by the



J6993

Figure 38 Spatial Beam Profile Influence on Raman Output

TABLE 3

LASER BEAM QUALITY IMPROVEMENTS HAVE RESULTED IN
ENHANCED S₂ PRODUCTION

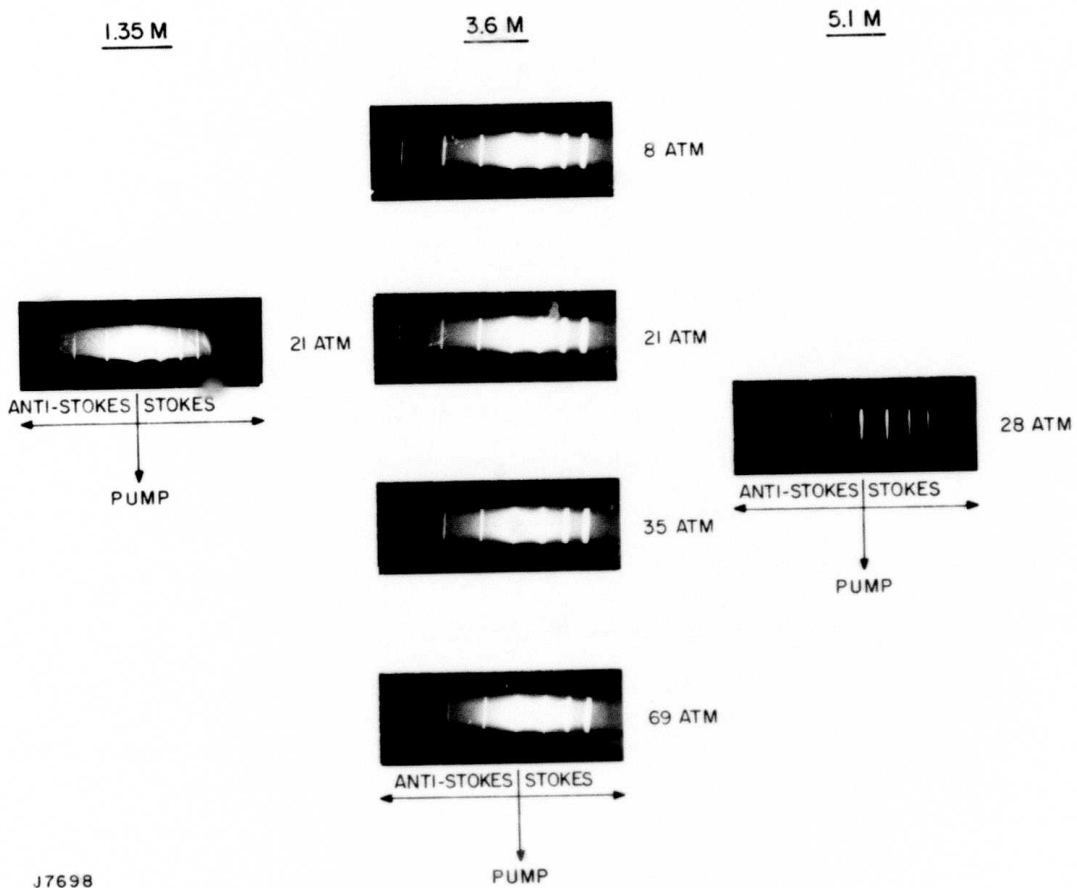
<u>OLD</u>		<u>NEW</u>
~1.2 J	ENERGY INTO RAMAN CELL	~1.2 J
~6 XDL	BEAM QUALITY	~2 XDL
≥70%	OVERALL CONVERSION EFFICIENCY	≥ 70%
~0.7	$\frac{S_2}{S_1}$ RATIO	~1.35
~25%	$\frac{\text{BLUE-GREEN OUT}}{\text{XeF IN}} * 100$	35%

⇒ CORRESPONDS TO
0.4 J IN 0.4 μsec

J7011

beam quality of the device, and the fact that these experiments utilize a focused beam.

In summary, experiments on a 10 mJ, 6 ns device showed significant conversion (66%) to S_1 could be achieved using XeF as a pump. Scaling these results to a 1 - 2 J, 400 ns, 1 m scale size device was reasonably straightforward and showed the importance of eliminating parametric processes for Raman control which was achieved by going to very soft focal beam experiments (see Figure 39). Also, over 70% (energy) pump depletion was routinely observed. This degree of conversion is consistent with the nature of the pump spatial beam quality and the qualitative far field intensity distribution discussed earlier.



J7698

Figure 39 Spectrographic Evidence for Focal Length Influence on Minimizing Parametric Processes

SECTION II

REFERENCES

1. Murray, J.R. and Javan, A., J. Molec. Spectry. 42, 1, (1972).
2. See for example: Minck, R.W., Terhune, R.W. and Rado, W.G., App. Phys. Lett. 3, 181, (1963), Demartini, F., and Ducuing, J., Phys. Rev. Lett. 17, 117 (1966), Bloembergen, N., Bret, G., Lallemand, P., Pine, A. and Sinova, P., IEEE J. of Quan. Elect. QE-3, 197 (1967), Venkin, G.V., Kulyuk, L.L. and Maleev, D.I., Sov. J. Quant. Electron 5, 1348 (1976), Loree, T.R., Sze, R.L., and Barker, D.L., App. Phys. Lett 31, 37 (1977), Wilke, V., and Schmidt, W., App. Phys. 18 177 (1979), Komine, H. and Stappaerts, E.A., Optics Lett. 4, 398 (1979) and Trainor, D.W., Hyman, H.A., Itzkan, I. and Heinrichs, R.M., App. Phys. Lett 37, 440 (1980).
3. Murray, J.R., Goldhar, J., Emerl, D., and Szoke, A., IEEE J. of Quant. Elect. QE-15, 342 (1974).
4. von der Linde, D., Maier, M. and Kaiser, W., Phys. Rev. 178, 178 (1969).
5. Zhdanov, B.V., Kulyuk, L.L. and Pershin, S.M., Sov. J. Quant. Electron 6, 550 (1976).
6. Barker, D.L. and Loree, T.R., Appl. Opt. 16, 1192 (1977).
7. Loree, T.R., Sze, R.C. and Barker, D.L., App. Phys. Lett. 31, 37 (1977).
8. Bloembergen, H., Bret, G., Lallemand, P., Pine, A. and Simova, P., IEEE J. Quant. Electron 3, 197 (1967).
9. Goldhar, J., Dickie, J., Bradley, L.P. and Pleasance, L.D., App. Phys. Lett. 31, 677 (1977).
10. Grasiuk, A., Private Communication (Dec. 1978).
11. Komine, H. and Stappaerts, E.A., Optics Lett. 4, 348 (1979).

DISTRIBUTION LIST

Office of Naval Research, Department of the Navy, Arlington, VA 22217 - Attn: Physics Program (1 copy)
 Naval Research Laboratory, Department of the Navy, Washington, D.C. 20375 - Attn: Technical Library (1 copy)
 Office of the Director of Defense, Research and Engineering, Information Office Library Branch, The Pentagon
 Washington, D.C. 20301 - (1 copy)
 U.S. Army Research Office, Box CM, Duke Station, Durham, N.C. 27706 - (1 copy)
 Defense Documentation Center, Cameron Station, Alexandria, VA 22314 - (1 copy)
 Defender Information Analysis Center, Battelle Memorial Institute, 505 King Avenue, Columbus, OH 43201 - (1 copy)
 Commanding Officer, Office of Naval Research Branch Office, 536 South Clark Street, Chicago, IL 60615 - (1 copy)
 New York Area Office, Office of Naval Research, 715 Broadway (5th Floor), New York, NY 10003 -
 Attn: Dr. Irving Rowe (1 copy)
 Air Force Office of Scientific Research, Department of the Air Force, Washington, D.C. 22209 - (1 copy)
 Office of Naval Research Branch Office, 1030 East Green Street, Pasadena, CA 91106 - Attn: Dr. Robert Behringer
 (1 copy)
 Defense Advanced Research Projects Agency, 1400 Wilson Blvd., Arlington, VA 22209 - Attn: Strategic Technology
 Office (1 copy)
 Office Director of Defense, Research and Engineering, The Pentagon, Washington, D.C. 20301 - Attn: Asst. Dir.
 (Space and Adv. Systems) (1 copy)
 Office of the Assistant Secretary of Def., System Analysis (Strategic Programs), Washington, D.C. 20301 -
 Attn: Mr. Gerald R. McNichols
 U.S. Arms Control and Disarmament Agency, Dept. of the State Bldg., Rm. 4931, Washington, D.C. 20451 Attn: Dr. Charles Henkin - (1 copy)
 Energy Research Development Agency, Division of Military Applications, Washington, D.C. 20545 - (1 copy)
 National Aeronautics and Space Admin., Lewis Research Center, Cleveland, Oh 44135 - Attn: Dr. John W. Dunning, Jr.
 Aerospace Research Engineer
 (1 copy)
 National Aeronautics & Space Admin., Code RR, FOB 10B, 600 Independence Ave., SW, Washington, D.C. 20546 - (1 copy)
 National Aeronautics and Space Admin., Ames Research Center, Moffitt Field, CA 94035 - Attn: Dr. Kenneth W. Billman
 (1 copy)
 Department of the Army, Office of the Chief of RD&A, Washington, D.C. 20310 - Attn: DARD-DD (1 copy)
 Department of the Army, Office of the Chief of RD&A, Washington, D.C. 20310 - Attn: DAMA-WSM-T (1 copy)
 Department of the Army, Office of the Deputy Chief of Staff for Operations and Plans, Washington, D.C. 20310
 Attn: DAMO-RQD (1 copy)
 U.S. Army Missile Command, Research and Development Division, Redstone Arsenal, AL 35809 - Attn: Army High
 Energy Laser Programs (1 copy)
 Commanding Officer, U.S. Army Mobility Equipment R&D Center, Ft. Belvoir, VA 22060 - Attn: SMEFB-MW (1 copy)
 Commander, U.S. Army Armanent Command, Rock Island, IL 61201 - Attn: AMSAR-RDT (1 copy)
 Director, Ballistic Missile Defense Adv. Technology Center, P.O. Box 1500, Huntsville, AL 35807 -
 Attn: ATC-O (1 copy)
 Director, Ballistic Missile Defense Adv. Technology Center, P.O. Box 1500, Huntsville, AL 35807 -
 Attn: ACT-T
 Commanding General, U.S. Army Munitions Command, Dover, NH 17801 - Attn: Mr. Gilbert F. Chesnov (AMSMU-R) (1 copy)
 Director, U.S. Army Ballistics Res. Lab., Aberdeen Proving Ground, MD 21005 - Attn: Dr. Robert Eichenberger (1 copy)
 Commandant U.S. Army, Air Defense School, Ft. Bliss, TX 79916 - Attn: Air Defense Agency (1 copy)
 Commandant, U.S. Army, Air Defense School, Ft. Bliss, TX 79916 - Attn: ATSA-CTD-MS (1 copy)
 Commanding General, U.S. Army Combat Dev. Command, Ft. Belvoir, VA 22060 - Attn: Director of Material,
 Missile Div. (1 copy)
 Commander, U.S. Army Training and Doctrine Command, Ft. Monroe, VA 23651 - Attn: ATCD-CF (1 copy)
 Commander, U.S. Army Electronics Command, Ft. Monmouth, NJ 07703, Attn: AMSEL-CT-L, Dr. R.G. Buser (1 copy)
 Commander, U.S. Army Combined Arms Combat Dev. Act., Ft. Leavenworth, KS 66027 - (1 copy)
 National Security Agency, Ft., Geo. G. Meade, MD 20755 - Attn: R.C. FOSS A763 (1 copy)
 Deputy Commandant - For Combat and Training Developments, U.S. Army Ordnance Center and School,
 Aberdeen Proving Ground, MD 21005 - Attn: ATSL-CTD-MS-R (1 copy)
 Department of the Navy, Office of the Chief of Naval Operations, The Pentagon 50739, Washington, D.C. 20350 -
 Attn: (OP 982F3)
 Boston Branch Office, Bldg. 114, Section D, 666 Summer Street, Boston, MA 02210 (1 copy)
 Department of the Navy, Deputy Chief of Navy Material (Dev.), Washington, D.C. 20360 -
 Attn: Mr. R. Gaylord (MAT 032B) (1 copy)
 Naval Missile Center, Point Mugu, CA 93042 - Attn: Gary Gibbs (Code 5352) (1 copy)
 Naval Research Laboratory, Washington, D.C. 20375 - Attn: Electro Optical Technology, Program Office,
 Code 1409 (1 copy)
 Naval Research Laboratory, Washington, D.C. 20375 - Attn: Dr. P. Livingston - Code 5560 (1 copy)
 Naval Research Laboratory, Washington, D.C. 20375 - Attn: Dr. A.I. Schindler - Code 6000 (1 copy)
 Naval Research Laboratory, Washington, D.C. 20375 - Attn: Dr. John L. Walsh - Code 5503 (1 copy)
 High Energy Laser Project Office, Department of the Navy, Naval Sea System Command, Washington, D.C. 20360 -
 Attn: Capt. A. Skolnick, USN (PM 22) (1 copy)
 Superintendent, Naval Postgraduate School, Monterey, CA 93940 - Attn: Library (Code 2124) (1 copy)
 Navy Radiation Technology, Air Force Weapons Lab (NLO), Kirtland AFB, NM 87117 (1 copy)
 Naval Surface Weapons Center, White Oak, Silver Spring, MD 20910 - Attn: Dr. Leon H. Schindel
 (Code 310) (1 copy)

DISTRIBUTION LIST (Continued)

Naval Surface Weapons Center, White Oak, Silver Spring, MD 20910 - Attn: Dr. E. Leroy Harris (Code 313) (1 copy)
 Naval Surface Weapons Center, White Oak, Silver Spring, MD 20910 - Attn: Mr. K. Enkenhaus (Code 034) (1 copy)
 Naval Surface Weapons Center, White Oak, Silver Spring, MD 20910 - Attn: Mr. J. Wise (Code 047) (1 copy)
 Naval Surface Weapons Center, White Oak, Silver Spring, MD 20910 - Attn: Technical Library (1 copy)
 U.S. Naval Weapons Center, China Lake, CA 93555 - Attn: Technical Library (1 copy)
 HQ AFSC/XRLW, Andrews AFB, Washington, D.C. 20331 - Attn: Maj. J.M. Walton (1 copy)
 HQ AFSC (DLCAW), Andrews AFB, Washington, D.C. 20331 - Attn: Maj. H. Axelrod (1 copy)
 Air Force Weapons Laboratory, Kirtland AFB, NM 87117 - Attn: LR (1 copy)
 Air Force Weapons Laboratory, Kirtland AFB, NM 87117 - Attn: AL (1 copy)
 HQ Aeronautical Systems Div., Wright Patterson AFB, OH 45433 - Attn: WRF - Mr. Clifford Fawcett (1 copy)
 Rome Air Development Command, Griffiss AFB, Rome, NY 13440 - Attn: Mr. R. Urtz (OCSE) (1 copy)
 HQ Electronics Systems Div. (ESL), L.G. Hanscom Field, Bedford, MA 01730 - Attn: Mr. Alfred E. Anderson (XRT) (1 copy)
 HQ Electronics Systems Div. (ESL), L.G. Hanscom Field, Bedford, MA 01730 - Attn: Technical Library (1 copy)
 Air Force Rocket Propulsion Lab., Edwards AFB, CA 93523 - Attn: B.R. Bornhorst, (LKCG) (1 copy)
 Air Force Aero Propulsion Lab., Wright Patterson AFB, OH 45433 - Attn: Col. Walter MOE (CC) (1 copy)
 Dept. of the Air Force, Foreign Technology Division, Wright Patterson AFB, OH 45433 - Attn: PDTN (1 copy)
 Commandant of the Marine Corps., Scientific Advisor (Code RD-1), Washington, D.C. 20380 (1 copy)
 Aerospace Research Labs., (AP), Wright Patterson AFB, OH 45433 - Attn: Lt. Col. Max Duggins (1 copy)
 Defense Intelligence Agency, Washington, D.C. 20301 - Attn: Mr. Seymour Berler (DTIB) (1 copy)
 Central Intelligence Agency, Washington, D.C. 20505 - Attn: Mr. Julian C. Nall (1 copy)
 Airesearch Manuf. Co., 9851-9951 Sepulveda Blvd., Los Angeles, CA 90009 - Attn: Mr. A. Colin Stancliffe (1 copy)
 Atlantic Research Corp., Shirley Highway at Edsall Road, Alexandria, VA 22314 - Attn: Mr. Robert Naismith (1 copy)
 Battelle Columbus Laboratories, 505 King Avenue, Columbus, OH 43201 - Attn: Mr. Fed Tietzel (STPIAC) (1 copy)
 Bell Aerospace Co., Buffalo, NY 14240 - Attn: Dr. Wayne C. Solomon (1 copy)
 Boeing Company, P.O. Box 3999, Seattle, WA 98124 - Attn: Mr. M.I. Gamble (2-,460,MS 8C-88) (1 copy)
 Electro-Optical Systems, 300 N. Halstead, Pasadena, CA 91107 - Attn: Dr. Andrew Jensen (1 copy)
 General Electric Co., Space Division, P.O. Box 8555, Philadelphia, PA 19101 - Attn: Dr. R.R. Sigismonti (1 copy)
 General Electric Co., 100 Plastics Avenue, Pittsfield, MA 01201 - Attn: Mr. D.G. Harrington (Rm. 1044) (1 copy)
 Hercules, Inc., Industrial Dept., Wilmington, DE 19899 - Attn: Dr. R.S. Voris (1 copy)
 Hercules, Inc., P.O. Box 210, Cumberland, MD 21502 - Attn: Dr. Ralph R. Preckel (1 copy)
 Hughes Research Labs., 3011 Malibu Canyon Road, Malibu, CA 90265 - Attn: Dr. D. Forster (1 copy)
 Hughes Aircraft Co., Aerospace Group-Systems Division, Canoga Park, CA 91304 - Attn: Dr. Jack A. Alcalay (1 copy)
 Hughes Aircraft Co., Centinela and Teale Streets, Building 6, MS E-125, Culver City, CA 90230 -
 Attn: Dr. William Yates (1 copy)
 Institute for Defense Analyses, 400 Army-Navy Drive, Arlington, VA 22202 - Attn: Dr. Alvin Schnitzler (1 copy)
 Lawrence Livermore Laboratory, P.O. Box 808, Livermore, CA 94550 - Attn: Dr. R.E. Kidder (1 copy)
 Lawrence Livermore Laboratory, P.O. Box 808, Livermore, CA 94550 - Attn: Dr. E. Teller (1 copy)
 Lawrence Livermore Laboratory, P.O. Box 808, Livermore, CA 94550 - Attn: Dr. Joe Fleck (1 copy)
 Los Alamos Scientific Laboratory, P.O. Box 1663, Los Alamos, NM 87544 - Attn: Dr. Keith Boyer (1 copy)
 Lockheed Palo Alto Research Lab., 3251 Hanover Street, Palo Alto, CA 94303 - Attn: L.R. Lunsford,
 Orgn. 52-24, Bldg. 201 (1 copy)
 Mathematical Sciences Northwest, Inc., P.O. Box 1887, Bellevue, WA 98009 - Attn: Dr. Abraham Hertzberg (1 copy)
 Massachusetts Institute of Technology, Lincoln Laboratory, P.O. Box 73, Lexington, MA 02173 -
 Attn: Dr. S. Edelberg (1 copy)
 Massachusetts Institute of Technology, Lincoln Laboratory, P.O. Box 73, Lexington, MA 02173 -
 Attn: Dr. L.C. Marquet (1 copy)
 McDonnell Douglas Astronautics Co., 5301 Bolsa Avenue, Huntington Beach, CA 92647 -
 Attn: Mr. P.L. Klevatt, Dept. A3-830-BBFO, M/Sg (1 copy)
 McDonnell Douglas Research Labs., Dept. 220, Box 516, St. Louis, MO 63166 - Attn: Dr. D.P. Ames (1 copy)
 Dr. Anthony N. Pirri, 30 Commerce Way, Woburn, MA 01801 (1 copy)
 Rand Corp., 1700 Main Street, Santa Monica, CA 90406 - Attn: Dr. C.R. Culp/Mr. G.A. Carter (1 copy)
 Raytheon Co., 28 Seyon Street, Waltham, MA 02154 - Attn: Dr. F.A. Horrigan (Res. Div.) (1 copy)
 Raytheon Co., Boston Post Road, Sudbury, MA 01776 - Attn: Dr. C. Sonnenschien (Equip. Div.) (1 copy)
 Raytheon Co., Bedford Labs, Missile Systems Div., Bedford, MA 01730 - Attn: Dr. H.A. Mehlhorn (1 copy)
 Riverside Research Institute, 80 West End Street, New York, NY 10023 - Attn: Dr. L.H. O'Neill (1 copy)
 Riverside Research Institute, 80 West End Street, New York, NY 10023 - Attn: Dr. John Bose (1 copy)

DISTRIBUTION LIST (Continued)

Riverside Research Institute, 80 West End Street, New York, NY 10023 - Attn: (NBSGL Library) (1 copy)

Rockwell International Corporation, Rocketdyne Division, Albuquerque District Office, 3636 Manaul Blvd.,
 Me, Suite 211, Albuquerque, NM 87110 - Attn: C.K. Kraus, NGR. (1 copy)

Sandia Corp., P.O. Box 5800, Albuquerque, NM 87115 - Attn: Dr. Al Marath (1 copy)

Stanford Research Institute, Menlo Park, CA 94025 - Attn: Dr. F.T. Smith (1 copy)

Science Applications, Inc., 1911 N. Ft. Meyer Drive Arlington, VA 22209 - Attn: L. Peckham (1 copy)

Science Applications, Inc., P.O. Box 328, Ann Arbor, MI 48103 - Attn: R.E. Meredith (1 copy)

Science Applications, Inc., 6 Preston Court, Bedford, MA 01703 - Attn: R. Greenberg (1 copy)

Science Applications, Inc., P.O. Box 2351, La Jolla, CA 92037 - Attn: Dr. John Amus (1 copy)

Systems Science and Software, P.O. Box 1620, La Jolla, CA 92037 - Attn: Alan F. Klein (1 copy)

Systems Consultants, Inc., 1050 31st Street, NW, Washington, D.C. 20007 - Attn: Dr. R.B. Keller (1 copy)

Thiokol Chemical Corp., Wasatch Division, P.O. Box 524, Brigham City, UT 84302 - Attn: Mr. J.E. Hansen (1 copy)

TW Systems Group, One Space Park, Bldg. R-1, Rm. 1050, Redondo Beach, CA 90278 - Attn: Mr. Norman Campbell (1 copy)

United Technologies Research Center, 400 Main Street, East Hartford, CT 06108 - Attn: Mr. G.H. McLafferty (1 copy)

United Technologies Research Center, Pratt and Whitney Aircraft Div., Florida R&D Center, West Palm Beach, FL 33402,
 Attn: Dr. R.A. Schmidke (1 copy)

United Technologies Research Center, Pratt and Whitney Aircraft Div., Florida R&D Center, West Palm Beach, FL 33402,
 Attn: Mr. Ed Pinsky

Varian Associates, EIMAC Division, 301 Industrial Way, San Carlos, CA 94070 - Attn: Mr. Jack Quinn (1 copy)

Vought Systems Division, LTV Aerospace Corp., P.O. Box 5907, Dallas, TX 75222 - Attn: Mr. F.G. Simpson, MS254142
 (1 copy)

Westinghouse Electric Corp., Defense and Space Center, Balt-Wash. International Airport, Box 746,
 Baltimore, MD 21203 - Attn: Mr. W.F. List (1 copy)

Westinghouse Research Labs., Baulah Road, Churchill Boro, Pittsburgh, PA 15235 - Attn: Dr. E.P. Riedel (1 copy)

United Technologies Research, East Hartford, CT 06108 - Attn: A.J. DeMaria (1 copy)

Aireborne Instruments Laboratory, Walt Whitman Road, Melville, NY 11746 - Attn: F. Pace (1 copy)

General Electric R&D Center, Schenectady, NY 12305 - Attn: Dr. Donald White (1 copy)

Cleveland State University, Cleveland, OH 44115 - Attn: Dean Jack Soules (1 copy)

Exxon Research and Engineering Co., P.O. Box 8 Linden, NJ 07036 - Attn: D. Grafstein (1 copy)

University of Maryland, Department of Physics and Astronomy, College Park, MD 20742 - Attn: D. Currie (1 copy)

Sylvania Electric Products Inc., 100 Ferguson Drive, Montian View, CA 94040 - Attn: L.M. Osterink (1 copy)

North American Rockwell Corp., Autonetics Division, 3370 Miraloma Avenue, Anaheim, CA 92803 -
 Attn: R. Gudmundsen (1 copy)

Massachusetts Institute of Technology, 77 Massachusetts Avenue, Cambridge, MA 02138 - Attn: Prof. A. Javan (1 copy)

Lockheed Missile & Space Co., Palo Alto Research Laboratories, Palo Alto, CA 94304 - Attn: Dr. R.C. Ohlman (1 copy)

Polytechnic Institute of New York, Rt. 110, Farmingdale, NY 11735 - Attn: Dr. William T. Walter (1 copy)